Palmitoylation Dynamics in Cell Division

by

Gamze Nur Yapıcı

A Dissertation Submitted to the
Graduate School of Sciences and Engineering
in Partial Fulfillment of the Requirements for
the Degree of

Master of Science

in

Molecular Biology and Genetics

KOÇ ÜNİVERSİTESİ

July 30, 2025

Palmitoylation Dynamics in Cell Division

Koç University

Graduate School of Sciences and Engineering

This is to certify that I have examined this copy of a master's thesis by

Gamze Nur Yapıcı

and have found that it is complete and satisfactory in all respects,
and that any and all revisions required by the final
examining committee have been made.

Committee Members:

_____

Prof. Nurhan Özlü

_____

Prof. Mutay Aslan

_____

Asst. Prof. Eda Yıldırım

Date: _____

To the younger me, who started this journey

ABSTRACT

Palmitoylation Dynamics in Cell Division
Gamze Nur Yapıcı
Master of Science in Molecular Biology and Genetics
July 30, 2025

The cell cycle is mainly regulated by post-translational modifications. While phosphorylation is well-established regulator of the cell cycle progression, the role of palmitoylation in this process has not been systematically characterized. This thesis investigates the regulatory role of palmitoylation in the cell cycle. To profile dynamic palmitoylation changes this study combines SILAC-based metabolic labeling with click chemistry. HeLa cells were labelled with heavy and light isotopes and synchronized to mitosis and interphase, respectively. After metabolic labeling with 17-ODYA, palmitoylated proteins are biotinylated by click chemistry and enriched using streptavidin pulldown. Quantitative analysis identified 3,239 proteins, 741 of which showed significant changes in palmitoylation between interphase and mitotic cells. Among these, 381 proteins are enriched as mitosis selective and 360 as interphase selective palmitoylated proteins. Furthermore, quantitative analysis identifies 2678 proteins in cells synchronized at mitosis and cytokinesis. Among these, palmitoylation of 83 proteins are significant in mitosis while 109 proteins are significant in cytokinesis. The results suggest that palmitoylation is regulated in a cell cycle-dependent manner. RNAi-based functional screening identifies ZDHHC5 as a key regulator of cell division, with its depletion resulting in prolonged cytokinesis and an increase in multinucleated cell rate. A remarkable crosstalk between palmitoylation and phosphorylation is observed. The most significant interaction between palmitoylation and phosphorylation is observed in mitotic proteins. The mitosis-selective cluster (Cluster 4) is identified as the largest cluster in the phosphoproteome dataset [Karayel et al., 2018]. Cluster 4 is most enriched in proteins that are likely co-regulated by both palmitoylation and phosphorylation. A CRISPR/Cas9 mediated *ZDHHC5* knockout (KO) cell line was constructed to investigate its enzymatic role during cytokinesis. Label-free quantitative proteomics analysis of the KO cells identified 210 potential candidate substrates of ZDHHC5 at cytokinesis.

The findings indicate a potential role for lipid-based modifications in coordinating cell division mechanisms.

ÖZETÇE

Hücre Bölünmesi Sürecinde Palmitolasyon Dinamikleri
Gamze Nur Yapıcı
Moleküler Biyoloi ve Genetik, Yüksek Lisans
Temmuz 2025

Hücre döngüsü başlıca translasyon sonrası modifikasyonlarla düzenlenir. Fosforilasyon, hücre döngüsü ilerleyişinin en iyi bilinen bir düzenleyicisi olsa da, palmitolasyonun bu süreçteki rolü sistematik olarak karakterize edilmemiştir. Bu tez, hücre döngüsünde palmitoilasyonun düzenleyici rolünü araştırmaktadır. Dinamik palmitoilasyon değişimlerini profillemek için çalışma, SILAC tabanlı metabolik işaretlemeyi klik kimyası ile birleştirmektedir. HeLa hücreleri, ağır ve hafif izotoplarla etiketlenmiş ve sırasıyla mitoz ve interfaz evrelerine senkronize edilmiştir. 17-ODYA ile metabolik olarak işaretlendikten sonra, palmitole proteinler klik kimyası aracılığıyla biyotinlenmiş ve streptavidin zenginleştirilme yöntemiyle çöktürülmüştür. Kantitatif analizde 3239 protein tanımlanmış, bunlardan 741'inde interfaz ve mitotik hücreler arasında anlamlı palmitolasyon değişiklikleri saptanmıştır. Bu proteinlerin 381'i mitoz-selektif, 360'ı ise interfaz-selektif palmitole proteinler olarak tanımlanmıştır. Ayrıca, mitoz ve sitokineze senkronize edilmiş hücrelerde 2,678 protein tanımlanmıştır. Bu proteinlerden 83'ünün mitozda, 109'unun ise sitokinezde anlamlı düzeyde palmitoillenmiş olduğu belirlenmiştir. Elde edilen sonuçlar, palmitoilasyonun hücre döngüsüne bağlı şekilde düzenlendiğini göstermektedir. RNAi tabanlı fonksiyonel tarama, ZDHHC5'in hücre bölünmesinde kilit bir düzenleyici olduğunu ortaya koymuştur; bu enzimin eksikliği, sitokinezin uzamasına ve çok çekirdekli hücre oranında artışa yol açmaktadır. Ayrıca, palmitoilasyon ile fosforilasyon arasında dikkat çekici bir karşılıklı etkileşim gözlemlenmiştir. Bu etkileşim en belirgin şekilde mitotik proteinlerde görülmüştür. Fosfoproteom verisinde yer alan en büyük küme olan mitoz-selektif Küme 4 (Cluster 4), palmitoilasyon ve fosforilasyon tarafından birlikte düzenlenmesi muhtemel proteinler açısından en zengin kümedir [Karayel et al., 2018]. Sitokinez sırasında ZDHHC5'in enzimatik rolünü araştırmak üzere CRISPR/Cas9 aracılığıyla *ZDHHC5* gen silinmiş hücre hattı oluşturulmuştur. Bu hücrelerde yapılan etiketsiz kantitatif proteomik analiz, sitokinezde ZDHHC5'in 210 potansiyel hedef

substratını tanımlamıştır. Bulgular, lipid tabanlı modifikasyonların hücre bölünmesi mekanizmalarını koordine etmede potansiyel bir rol oynadığını göstermektedir.

ACKNOWLEDGMENTS

First and foremost, I would like to express my deepest gratitude to my advisor, Prof. Dr. Nurhan Özlü, for her invaluable guidance, scientific insight, and constant support throughout the course of this thesis. Her mentorship has played a crucial role in shaping my academic development and scientific perspective.

I would also like to thank the members of my thesis jury, Prof. Dr. Mutay Aslan and Asst. Dr. Eda Yıldırım for kindly accepting to evaluate my thesis and participate in the defense.

I am especially thankful to Dr. Nazlı Ezgi Özkan, from whom I learned almost every technique and experiment used in this thesis. She always approached me with patience and clarity, supported me without limitations, and was my greatest academic mentor throughout. Beyond that, she made me feel like family. I truly believe she was the best colleague I could have worked with on this project, and I feel incredibly lucky for that.

My sincere thanks go to the members of the Nozlu Lab for providing a supportive research environment. I'm also deeply thankful to Büşra, whose calm support and thoughtful advice always made tough moments easier. Although we worked on different projects, Dr. Beste Senem was always one of the first people I turned to for scientific discussions and her insight and friendship were truly appreciated. I would like to thank Danny for his support whenever I needed help during my analyses. My friendship with Dilaray and Hale is one of the things I'll always cherish from my time at Koç University both of them made the hard days easier and the good days more fun. Many thanks to Asiye and İnci for being there with their kindness and friendship. I am especially grateful to İnci for joining the project in its final stages and offering her support when it was most needed.

I'm especially grateful to Ferdi Güler, my closest friend since 11 years. Over the

years, his constant presence has not only supported me through every challenge but also strengthened the bond we share one that feels more like a brotherhood to me than friendship. Sharing dreams and late-night talks about life and the future have made our friendship feel truly real.

The most precious person Koç University brought into my life is Enes Ulaş Dinçer, my boyfriend and also my best friend. You are truly one of the most principled and admirable people I've ever known, and I feel incredibly lucky to have you in my life. Along the way, we've shared countless memories, both sweet and difficult, and now, as two PhD candidates, we're stepping into a new chapter of our lives together. Your steady belief in me and quiet strength have carried me through every analysis, presentation, and challenge. Your support has been constant and deeply felt. And I hope that every day we share from now on carries the depth, warmth, and quiet beauty that "Süreya" means to us.

I would like to express my heartfelt gratitude to Nihal Nezir, Selma Çelik, and Ayşe Ertuğrul, three of the kindest souls I've ever known. Since my high school years, they've supported me in my academic journey and believed in me even at times when I couldn't see my own potential. My love and respect for them will always stay with me.

To my mother Pakize, whose sacrifices are countless. Over the years, I've come to see more of her in myself, and our bond has grown into something closer to friendship I value deeply. To my father Mahir, who probably loves me more than anyone in the world. I will never forget how you eagerly waited for weekends just so I could come home from the lab, often bringing sweets to celebrate my arrival. That meant everything to me. To my sister Sude, I'm so glad I insisted on you being born. Your wild spirit and unstoppable energy may make me seem like the calm and wise one, but the truth is, you inspire me more than you know. To my little brother Yiğit, my favorite "troublemaker" when I see you still diving into pools like nothing's changed, I realize some things thankfully stay the same. And I kind of hope they always do.

TABLE OF CONTENTS

LIST OF TABLES

LIST OF FIGURES

ABBREVIATIONS

17-ODYA	17-Octadecynoic Acid
APT	Acyl Protein Thioesterase
BFDR	Bayesian False Discovery Rate
CPC	Chromosomal Passenger Complex
DDA	Data-Dependent Acquisition
DHHC	Asp-His-His-Cys Motif
DMEM	Dulbecco's Modified Eagle Medium
DMSO	Dimethyl Sulfoxide
FASP	Filter Aided Sample Preparation
FBS	Fetal Bovine Serum
FDR	False Discovery Rate
GFP	Green Fluorescent Protein
GO	Gene Ontology
KO	Knockout
LC-MS/MS	Liquid Chromatography Tandem Mass Spectrometry
LFQ	Label-Free Quantification
NCE	Normalized Collision Energy
NT	Non-Targeting
PBS	Phosphate-Buffered Saline
PIP_2	Phosphatidylinositol phosphate
PLA	Proximity Ligation Assay
PSM	Peptide Spectrum Match
PTM	Post-Translational Modification
SILAC	Stable Isotope Labeling by Amino Acids in Cell Culture

sgNT	Single Guide Non-Targeting
STLC	S-trityl-L-cysteine
TCEP	Tris(2-carboxyethyl)phosphine
TMT	Tandem Mass Tag
ZDHHC	Zinc Finger DHHC-type Containing

Chapter 1

INTRODUCTION

Cell division is a fundamental biological process that allows cells to grow, multiply, and maintain healthy tissues. For cell division to proceed accurately, a series of tightly regulated events must occur in the correct sequence including DNA replication, chromosome segregation, cell shape remodeling, and membrane reorganization to form two distinct daughter cells. These steps are carefully coordinated by cellular machinery through both molecular and structural mechanisms.

One way cells manage this complex process is by modifying proteins after they are made. These modifications, known as post-translational modifications (PTMs), can affect how proteins work, how stable they are, and where they are located within the cell. Common examples of PTMs include phosphorylation, ubiquitination, acetylation, and lipidation, each playing distinct roles in regulating protein function. However, recent studies have pointed to the importance of lipid-based modifications, like palmitoylation, in regulating cell division as well.

Among these, lipid-based modifications such as palmitoylation have recently gained attention for their potential involvement in cell division. Palmitoylation involves the reversible attachment of a palmitate to proteins that influences their membrane association and activity. Although its role has been widely studied in the context of signaling and trafficking, the contribution of palmitoylation to mitosis and cytokinesis remains less well understood.

In this thesis, changes in protein palmitoylation during different stages of the cell cycle are explored in detail. A combination of stable isotope labeling by amino acids in cell culture (SILAC)-based metabolic labeling and click chemistry is used to identify palmitoylated proteins in interphase, mitosis, and cytokinesis. Additionally,

the enzyme ZDHHC5 which adds palmitate to proteins is studied to understand how it may contribute to the regulation of cell division.

Chapter 2

LITERATURE REVIEW

2.1 Cell Division

Cell division is a fundamental biological process required for the accurate segregation of genetic material and cytoplasmic components into daughter cells, hence ensuring the maintenance and propagation of life. Accurate distribution is also required for the internal parts of the cell, including the endoplasmic reticulum, mitochondria, and Golgi apparatus. These organelles undergo precisely timed remodelling events during each stage of mitosis instead of to simply splitting in half. Mitochondria dynamically fragment and reorganize, and the Golgi network splits and reorganizes into vesicles during division. These changes are driven by signalling pathways precisely. Cell viability may be affected if this coordination is disturbed, highlighting the critical role that organelle and membrane dynamics play in a successful division.

A highly controlled molecular machinery is responsible for the extensive structural remodeling that occurs in tandem with this event. Cell rounding, focal adhesion disassembly, actomyosin cortex assembly, changes in intracellular pressure and cell volume, and dynamic organelle repositioning are examples of distinctive morphological changes. Cell rounding, focal adhesion disintegration, actomyosin cortex assembly, changes in intracellular pressure and cell volume, and dynamic organelle repositioning are the morphological changes that are characteristic [Champion et al., 2017]. In addition to morphological changes, the protein composition of the cell surface is dynamically altered during cell cycle. For instance, surface proteomics analysis revealed that protocadherins, like PCDH7 and PCDH1, are mitosis-enriched surface proteins, suggesting that specific membrane proteins are controlled in their trafficking during division [Özlü et al., 2015].

2.2 Post-Translational Modifications

During the cell cycle, PTMs are crucial molecular processes that give cells precise and dynamic control over protein function. PTMs control where and when proteins act by adding small chemical groups or changing the structure of proteins, enabling cells to react rapidly to the demands of cytokinesis and mitosis.

PTMs are covalent modifications that occur in one or more amino acids of a protein after mRNA mediated translation, either through proteolytic cleavage or the addition of a modifying group. Although the human genome contains approximately 20,000 genes, the human proteome is much more complex, with more than a million distinct proteoforms. This complexity arises from various molecular mechanisms, including alternative splicing and PTMs. More than 400 distinct PTMs regulate protein function by altering the activity state, subcellular localization, turnover, protein-protein interactions, and molecular trafficking (Figure 2.1) [Ramazi and Zahiri, 2021].

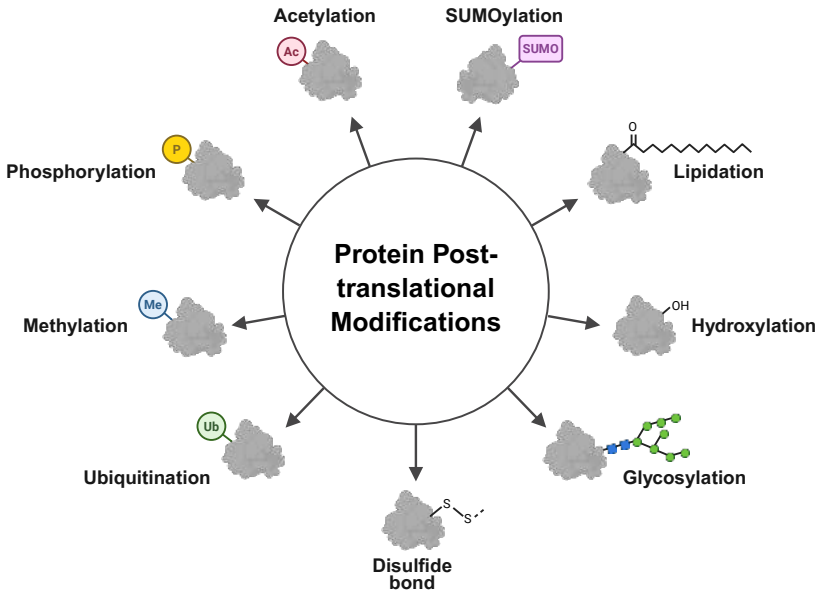

Figure 2.1: Schematic overview of major protein post-translational modifications (Created with BioRender.com.).

2.2.1 Phosphorylation

Phosphorylation represents one of the most extensively utilized and tightly controlled PTMs involved in the regulation of cell division. PTMs can be grouped into two categories based on their reversibility. Phosphorylation is the most prevalent reversible PTM, with a total of 1,775,640 annotated sites in the dbPTM database, including 1,615,150 experimentally validated sites and 160,490 putative sites, supported by 39,780 literature references [Chung et al., 2025].

Phosphorylation affects the activation state, stability, intracellular localization, and protein–protein interactions. It is mediated by the coordinated activity of kinases and phosphatases [Morgan, 2007]. Its regulatory importance extends beyond changes in protein expression, as evidenced by the 6,528 cell cycle-dependent phosphorylation events identified in large-scale phosphoproteomic studies, of which 5,464 occur independently of protein abundance [Rega et al., 2025]. These findings indicate that phosphorylation plays an important role by modulating protein function without altering protein levels.

A specific example is the phosphorylation of ERM (ezrin, radixin, and moesin) proteins, which couples actomyosin contractility to the plasma membrane during mitotic entry. The morphological change to a rounded shape and the successful progression of mitosis requires this phosphorylation event [Leguay et al., 2022].

Phosphorylation also functions as a molecular switch that ensures the timely execution of key mitotic processes, including chromosome condensation, spindle formation, nuclear envelope disassembly, and centrosome maturation [Olsen et al., 2010]. Core mitotic regulators, including cyclin-dependent kinases (CDKs), Polo-like kinases (PLKs), and Aurora kinases, depend on precise phosphorylation patterns to function properly [Petronczki et al., 2008, Nigg, 1993]. When phosphorylation dynamics are misregulated, the fidelity of mitosis is disrupted, which can lead to chromosomal instability and disease states such as cancer.

2.3 Palmitoylation

S-palmitoylation has become a prominent lipid-based regulator among PTMs, particularly important for membrane dynamics during cell division. The reversible lipid PTM referred to as S-palmitoylation is defined by the covalent bonding of the 16-carbon saturated fatty acid palmitate to cysteine residues through a thioester bond. A family of palmitoyl acyltransferases (PATs), which usually have a conserved DHHC (Asp-His-His-Cys) motif, catalyse this dynamic modification and acyl-protein thioesterases (APTs) reverse it (Figure 2.2).

Protein half-life, trafficking pathways, membrane affinity, and subcellular localization are all affected by palmitoylation, which provides extensive regulatory control over protein behavior [Conibear and Davis, 2010]. When the proteins get palmitoylated, they associate with specific membrane compartments and rapidly reorganize in response to cellular signals. Unlike irreversible lipid modifications like myristoylation and prenylation, palmitoylation offers a flexibility that allows cycles of membrane attachment and detachment. Many proteins involved in immune responses, vesicular transport, synaptic plasticity, and signal transduction exhibit this alteration. Additionally, distrupted palmitoylation is linked to diabetes, cancer, and neurodegeneration,which demonstrates its physiological significance role [Yuan et al., 2024].

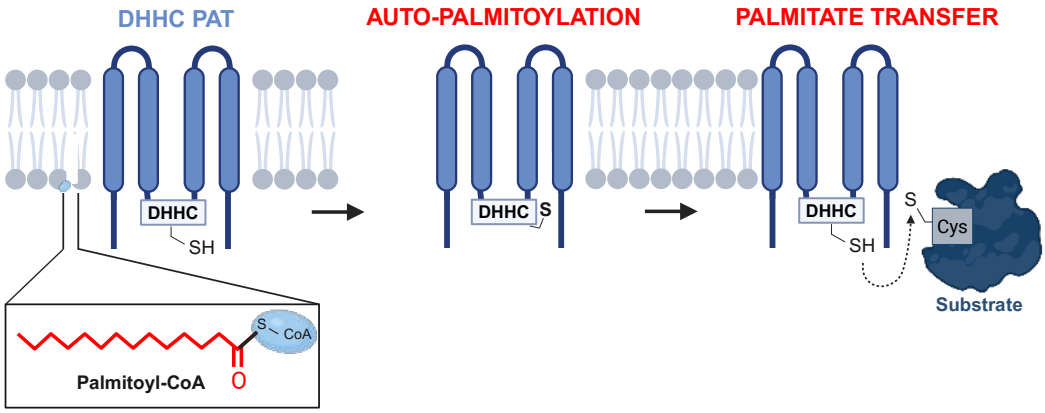

Figure 2.2: Schematic overview of major protein post-translational modification. Adapted from [Alonso-Matilla et al., 2024] (Created with BioRender.com.).

2.3.1 ZDHHC5 Enzyme Family

The conserved DHHC cysteine-rich domain necessary for catalytic activity is shared by all 23 palmitoyl acyltransferases in the human ZDHHC (zinc finger DHHC-type containing) family [Ohno et al., 2006]. These enzymes are transmembrane proteins that are primarily found in particular intracellular compartments, such as the plasma membrane (e.g., ZDHHC5, 20), Golgi apparatus (e.g., ZDHHC2, 7, 15, 17), and endoplasmic reticulum (e.g., ZDHHC1, 3, 6). Their substrate specificity are primarily dictated by their subcellular location [Greaves and Chamberlain, 2011]. Some ZDHHCs exhibit dynamic trafficking between compartments; for example, ZDHHC3 and ZDHHC7 cycle between the Golgi and plasma membrane, allowing for broader substrate access [Woodley and Collins, 2019]. Although there is some redundancy, each ZDHHC member frequently exhibits unique patterns of tissue expression and interacts with various scaffolds or adaptor proteins, which adds to regulatory diversity and substrate specificity [Ohno et al., 2006].

Being a constitutively plasma membrane-localized DHHC enzyme, ZDHHC5 can act on membrane-proximal substrates involved in cytoskeletal organization, membrane trafficking, and signal transduction [Plain et al., 2020]. Furthermore, ZD-

HHC5 has been demonstrated to translocate between the plasma membrane and endosomes through endocytic motifs in its C-terminal tail [Woodley and Collins, 2019]. ZDHHC5 is especially abundant in immune cells, neurons, and epithelial tissues, confirming its functions in immune signaling, synaptic plasticity, and epithelial polarity [Lemonidis et al., 2015]. Furthermore, ZDHHC5 activity is controlled by phosphorylation and substrate-dependent stabilization processes, which adjust its palmitoylating activity in response to cellular signals [Plain et al., 2020].

2.3.2 The role of palmitoylation in cell cycle regulation

Phosphorylation is the most studied PTM in cell cycle regulation. However, lipid modifications like palmitoylation have recently gained attention for their potential roles in cell division. While direct evidence is still emerging, several studies, as discussed below, highlight the involvement of palmitoylation in regulating mitotic processes. Lipid additions can influence membrane association, protein trafficking, and subcellular localization, which are particularly essenttial during cytokinesis [Atilla-Gokcumen et al., 2014]. Proteins and lipids accumulate at the cleavage furrow, and membrane remodeling is an important event in the plasma membrane during mitotic exit [Alonso-Matilla et al., 2024]. Reversible lipidation PTMs may be one of the coordinating mechanisms of cell division.

Palmitoylation plays a critical role in regulating distribution of proteins at key sites during cell division, including the cleavage furrow and the spindle apparatus [Conibear and Davis, 2010]. Several studies have shown that dynamic palmitoylation patterns influence membrane curvature, vesicle trafficking, and recruitment of scaffolding proteins to the mitotic cortex [Chamberlain and Shipston, 2015]. For instance, the accumulation of specific lipids and palmitoylated proteins at the cleavage furrow is essential for successful cytokinesis, where membrane elasticity and protein localization are tightly coordinated [Draper and Smith, 2009].

Lipids have several functions that are becoming more widely understood. These functions include lipid-based post-translational modifications, structural membrane components, and signalling molecules derived from lipids. Palmitoylation is becom-

ing increasingly recognised as an important driver of mitotic progression [Atilla-Gokcumen et al., 2014].

During cell division, palmitoylation facilitates regulatory proteins to localise selectively in the membrane. For instance, ZDHHC5 palmitoylates PCDH7, a modification necessary for appropriate furrow and cortical enrichment during mitosis [Özkan et al., 2023]. Beyond its role in directing membrane-associated proteins to the cleavage furrow, palmitoylation has been linked to a variety of processes in the regulation of mitosis in a wide range of organisms and environments. It has been demonstrated to play a regulatory role in the cytoskeleton by palmitoylating tubulin, which is necessary for proper nuclear migration during yeast mitosis [Linder and Deschenes, 2007]. A palmitoylation-dependent association between importin subunit α and the plasma membrane was discovered in the vertebrate system. This subunit is essential for nuclear transport and spindle size regulation. The reversible nature of the modification was revealed by the specific enhancement of membrane localisation that resulted from palmostatin-induced inhibition of depalmitoylation [Brownlee and Heald, 2019].

Additionally, palmitoylation seems to control asymmetric cell division. It has been demonstrated that the depalmitoylating enzyme APT1 interacts with the Rho GTPase CDC42 to control the distribution of polarised membranes in proteins like β-catenin and Numb [Stypulkowski et al., 2018]. These results suggest that palmitoylation afect the cortical polarity during mitosis.

Furthermore, for stable plasma membrane localisation and efficient signal transduction, the transmembrane protein CKAP4 needs DHHC2-mediated palmitoylation [Li et al., 2010]. Though the identities of these proteins have not yet been determined, palmitoylated proteins globally redistribute to the cleavage furrow during division, according to alkyne fatty acid-based imaging techniques [Hannoush and Arenas-Ramirez, 2009]. Furrow-localized palmitoyl-proteome datasets identified HRAS, NRAS, and RRAS among known palmitoylated signalling proteins, suggesting that lipid-modified small GTPases play a role in division-specific signalling [Rocks et al., 2010].

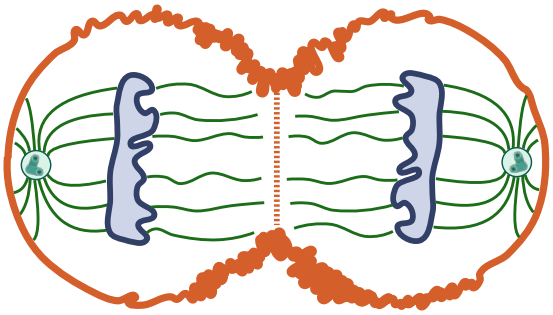

Figure 2.3: Schematic overview highlighting lipid accumulation in the cleavage furrow. Adapted from [Alonso-Matilla et al., 2024] (Created with BioRender.com.).

In this thesis, palmitoylation is proposed as a regulatory mechanism in the cell cycle. Metabolic labeling was performed using the alkyne-palmitate analogue 17-octadecynoic acid (17-ODYA). Subsequently, palmitoylated proteins were enriched through click chemistry. This enrichment process was coupled with SILAC-based quantitative mass spectrometry, enabling the generation of the first comprehensive dataset of cell cycle-resolved palmitoyl proteomes. Through this analysis, both known and previously unidentified palmitoylated proteins were detected, each exhibiting stage-specific enrichment patterns across interphase, mitosis, and cytokines.In addition, an RNAi screen was used to test which ZDHHC enzymes are important for cell division. This screen showed that ZDHHC5 is required for proper mitotic progression. To find the proteins that ZDHHC5 modifies, a ZDHHC5 knockout cell line was used. Proteomics analysis of these cells revealed potential ZDHHC5 substrates with reduced palmitoylation.

Chapter 3

MATERIALS AND METHODS

3.1 Cell Culture

HeLa Kyoto (a kind gift from Dr. Ulrike Eggert, Randall Centre for Cell and Molecular Biophysics, King's College London, UK) and HeLa S3 (ATCC CCL-2.2) cell lines were used. Cells were cultured in Dulbecco's Modified Eagle Medium (DMEM) supplemented with 10% heat-inactivated Fetal Bovine Serum (Advanced, South America; Techlabs Capricorn, FBS-HI-11A) or with SILAC dialyzed FBS (Medsantek Lifesciences, 26400044) for metabolic labeling experiments, 1% Penicillin/Streptomycin (Thermo, 15140122), and maintained at 37 °C in a humidified atmosphere with 5% CO_2. Each cell line was kept at 37 °C in a humidified incubator with 5% CO_2.

3.1.1 Stable Isotope Labeling by Amino Acids in Cell Culture

SILAC was used to quantitatively assess proteomic changes in palmitoylated proteins in different cell cycle stages. HeLa Kyoto cells were grown in SILAC DMEM medium lacking L-lysine and L-arginine (Thermo Fisher Scientific, Cat. No. 89985), supplemented with 10% dialyzed fetal bovine serum (Medsantek Lifesciences, Cat. No. 26400044), 1% Penicillin-Streptomycin (Thermo Fisher Scientific, Cat. No. 15140122), 200 mg/L L-proline (Sigma-Aldrich), and either unlabeled ("light") or isotope-labeled ("heavy") amino acids—L-lysine ($^{13}C_6$, $^{15}N_2$) and L-arginine ($^{13}C_6$, $^{15}N_4$) (Cambridge Isotope Laboratories).

Cells were cultured for at least six doublings to ensure complete incorporation of heavy amino acids. Culture medium was replaced every 2 to 3 days and cells were maintained at 70–80% confluency. Incorporation efficiency was assessed by LC-MS/MS analysis of cell lysates, and only cultures with higher than 95% labeling

efficiency were used in downstream proteomics experiments.

3.1.2 17-ODYA or Palmitic Acid Labeling

To metabolically label palmitoylated proteins, cells were incubated with 25 µM 17-ODYA (Cayman Chemical, Cat. No. 90270) or 25 µM palmitic acid (Alfa Aesar, Cat. No. B20322), each prepared as 25 mM stock solutions in DMSO (1000 ×). Prior to use, stock solutions were sonicated for at least 10 minutes to ensure complete solubilization.

Labeling reagents were added directly to the culture medium during the final stages of synchronization (e.g., during S-Trityl-L-cysteine treatment for mitotic arrest or Purvalanol A treatment for cytokinesis) and incubated under standard culture conditions. For SILAC experiments, labeling was performed in SILAC DMEM supplemented with dialyzed FBS (Medsantek Lifesciences, Cat. No. 26400044) and 1% Penicillin-Streptomycin.

3.2 Cell Cycle Synchronization and Verification

To obtain cell populations enriched in interphase, mitosis, or cytokinesis, synchronization protocols were applied to HeLa Kyoto, SILAC-labeled, and ZDHHC5-KO cells.

3.2.1 Double thymidine block for interphase arrest

Cells were treated with 2 mM thymidine (Sigma, Cat. No. T1895) for 20 hours, released into fresh medium for 7 hours, and then again treated with 2 mM thymidine for 20 hours. Cells were then harvested as either interphase-enriched or further processed for downstream synchronization.

3.2.2 STC based Mitotic arrest

To arrest cells in mitosis, the double thymidine block protocol was followed by release into fresh medium containing 10 µM STC (Alfa Aesar, Cat. No. L14384, 97%) for 16 hours. For experiments involving metabolic labeling of palmitoylated proteins,

cells were simultaneously incubated in labeling medium containing 25 µM 17-ODYA (Cayman Chemical, Cat. No. 90270) or 25 µM palmitic acid (Alfa Aesar, Cat. No. B20322). Mitotic cells were harvested by mitotic shake-off.

3.2.3 Purvalanol A induced monopolar cytokinesis

To induce monopolar cytokinesis, cells were first synchronized using a double thymidine block. Following release, cells were incubated with 10 μM STC for 6 hours to arrest them in mitosis. Without removing STC, 100 μM Purvalanol A (Sigma, Cat. No. P4485) was directly added to the culture medium, and cells were incubated for an additional 15 minutes at 37 °C (Figure 3.1). Cells were immediately harvested after treatment for further analysis.

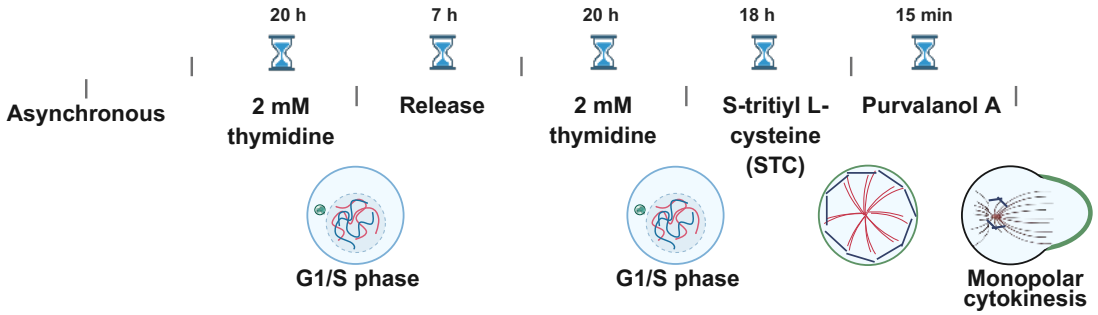

Figure 3.1: Experimental workflow of monopolar cytokinesis (Created with BioRender.com.).

3.2.4 Nocodazole-based bipolar cytokinesis and release protocol

To synchronize cells in bipolar cytokinesis, cells were first subjected to a double thymidine block. After release, cells were treated with 40 ng/mL nocodazole (Sigma, Cat. No. M1404) for 4 to 6 hours to arrest them in mitosis. Mitotic cells were then collected by mechanical shake-off and immediately released into fresh complete medium for approximately 1 hour to allow progression to bipolar cytokinesis prior to harvesting or fixation (Figure 3.2).

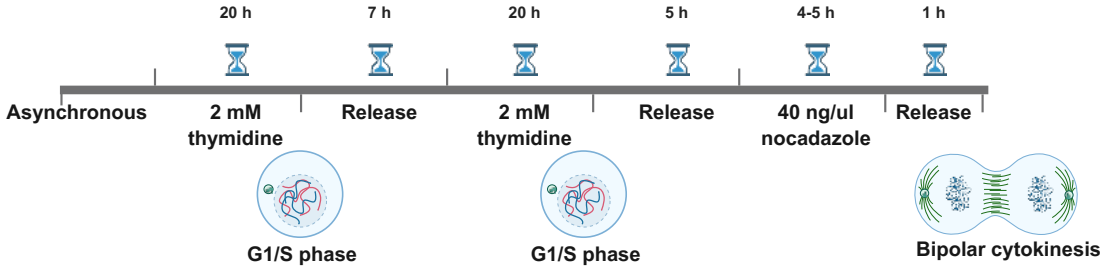

Figure 3.2: Experimental workflow of bipolar cytokinesis (Created with BioRender.com.).

3.2.5 Synchronization of HeLa Kyoto, SILAC-labeled, and ZDHHC5-KO cells for proteomic profiling

The three cell types, HeLa Kyoto, SILAC-labeled, and ZDHHC5-KO, were synchronized using the above protocols, depending on the experimental design. Synchronization was applied for comparative analysis of palmitoylation across cell cycle stages. Synchronization efficiency was verified using phase contrast microscopy to observe characteristic morphological features of each cell cycle phase.

3.3 Genetic and Pharmacological Manipulations

3.3.1 Palmitoylation inhibiton with 2-bromopalmitate

To inhibit protein palmitoylation, HeLa Kyoto cells were treated with 100 µM 2-bromopalmitate (2-BP; Sigma-Aldrich, Cat. No. 238422), a general inhibitor of palmitoyl acyltransferases. 2-BP was dissolved in DMSO and added to the culture medium for 16 hours prior to cell lysis or fixation. DMSO was used in control samples at equivalent volume. Following treatment, cells were either subjected to click chemistry labelling for palmitoylation detection or fixed for immunofluorescence microscopy.

3.3.2 siRNA-mediated knockdown of ZDHHC family members

To investigate the role of specific ZDHHC family members in palmitoylation-dependent processes such as multinucleation, HeLa cells were transiently transfected with ON-TARGETplus SMARTpool siRNAs targeting ZDHHC4, ZDHHC5, ZDHHC12, ZDHHC13, ZDHHC52, and ZDHHC524 (Horizon Discovery). A nontargeting siRNA pool was used as a negative control. Transfections were carried out using Lipofectamine™ RNAiMAX (Thermo Fisher Scientific, Cat. No. 13778150) in 24-well plates. Cells were seeded the day before transfection to reach approximately 60–70% confluency. For each well, 12 pmol of siRNA was diluted in 50 μl Opti-MEM® reduced Serum Medium and mixed with 1 μl Lipofectamine RNAiMAX also diluted in 59 μl Opti-MEM. After 15–20 minutes of incubation at room temperature, 100 μl of the siRNA-lipid complex was added dropwise to each well containing 400 μl of serum and antibiotic free DMEM. After 4 to 5 hours of incubation, the transfection medium was replaced with complete DMEM supplemented with 10% fetal bovine serum and antibiotics. A second transfection was performed 24 hours later to improve the knockdown efficiency. Cells were fixed 48 hours after the first transfection and processed for immunofluorescence microscopy. Knockdown efficiency was confirmed by immunoblotting or antibody staining.

3.3.3 CRISPR/Cas9-mediated knockout of ZDHHC5

gRNA Design and Cloning

To generate a stable knockout of the *ZDHHC5* gene, three different single-guide RNAs (sgRNAs) previously validated in the literature were selected. Complementary oligonucleotides corresponding to each sgRNA sequence were synthesized and phosphorylated using T4 Polynucleotide Kinase (New England Biolabs, Cat. No. M0201S).

The LentiCRISPR v2 plasmid (Addgene #52961) was linearized with BsmBI-v2 (New England Biolabs, Cat. No. R0739S) at 55 °C for 4 hours. To prevent religation of the plasmid backbone, the digested vector was treated with Antarctic Phosphatase (New England Biolabs, Cat. No. M0289S) and then heat-inactivated

at 80 °C. Digestion efficiency was confirmed by electrophoresis on a 1% agarose gel alongside an undigested control.

Phosphorylated oligonucleotides were annealed by incubation at 37 °C for 30 minutes, followed by heating at 95 °C for 5 minutes and gradual cooling to room temperature. The annealed oligos were ligated into the BsmBI-digested and dephosphorylated *LentiCRISPR v2* vector using T4 DNA Polymerase (Thermo Scientific, Cat. No. EP0061, Lot No. 00145676) in a 10 μl reaction, incubated at room temperature for 2 hours. Subsequently, $2-5\,\mu$l of the ligation product was transformed into DH5α competent *E. coli* via heat-shock at 42 °C for 45 seconds, followed by recovery in SOC medium at 37 °C for 1 hour. Transformed cells were plated on LB-agar containing 100 μg/mL ampicillin and incubated overnight. Individual colonies were picked for overnight culture in LB-ampicillin, and plasmids were purified using a miniprep kit (Macherey-Nagel) and verified by Sanger sequencing.

Transfection and Selection

Plasmid transfections were performed in HeLa Kyoto cells using Lipofectamine™ 3000 (Thermo Fisher Scientific) according to the manufacturer's protocol. Cells were seeded in 10 cm dishes to reach approximately 70–80% confluency on the day of transfection. For each dish, 7.5 µg of the expression construct (e.g., LentiCRISPR-v2 or pEF-BOS-HA-ZDHHC5) was mixed with Lipofectamine™ 3000 and P3000™ reagent in Opti-MEM™ I medium. The transfection mixture was added to cells in antibiotic-free DMEM supplemented with 10% FBS.

The medium was refreshed 6–8 hours after transfection. Cells were harvested 24 to 72 hours post-transfection for downstream assays. For stable selection, puromycin (1.5 µg/mL) was added 48 hours after transfection and maintained for 3–5 days. If needed, single-cell clones were isolated by limiting dilution, and ZDHHC5 expression levels were validated by Western blotting and immunofluorescence microscopy.

Confirmed sgRNA-containing LentiCRISPR constructs were transiently transfected into HeLa Kyoto cells using Lipofectamine™ 3000 (Thermo Fisher Scientific). Puromycin (1.5 µg/mL) selection was applied 24 hours after transfection and main-

tained for 48–72 hours to enrich cells successfully transfected. Bulk transfected populations were maintained in complete DMEM until further validation.

Clone Validation

Cells were diluted into 96-well plates for single-cell cloning after puromycin selection. Western blotting was used to verify ZDHHC5 expression in expanded clones. ZDHHC5-specific antibodies were used for immunofluorescence staining in order to further validate clones lacking the ZDHHC5 protein. For subsequent analyses, only clones with verified loss of ZDHHC5 protein were used. During every stage of validation, parental HeLa Kyoto cells and cells transfected with nontargeting sgRNAs were used as controls.

Table 3.1: Oligonucleotide sequences of sgRNAs targeting ZDHHC5, ZDHHC12, and ZDHHC13.

Oligonucleatide Name	**Oligonucleatide Sequence**
ZDHHC5 sg1 Forward [Ko et al., 2019]	5'-CACCGGAACCACGTGAAATCCCGTG–3'
ZDHHC5 sg1 Reverse [Ko et al., 2019]	5'-AAACCCACGGGATTTCACTGTGGTCC–3'
ZDHHC5 sg2 Forward [Sergeeva and van der Goot, 2019]	5'-CACCGAGGATACGTGAGACGCGTG–3'
ZDHHC5 sg2 Reverse [Sergeeva and van der Goot, 2019]	5'-AAACGCACGTCTCACGTATCCTC–3'
ZDHHC5 sg3 Forward [Gök et al., 2020]	5'-CACCGAGCTCCACTAGGAAGATGG–3'
ZDHHC5 sg3 Reverse [Gök et al., 2020]	5'-AAACCCATCTTCCTAGTGGAGCTC–3'
ZDHHC12 sg1 Forward [Wang et al., 2023]	5'-CACCGTGACCGACGTCCGACCCGC–3'
ZDHHC12 sg1 Reverse [Wang et al., 2023]	5'-AAACGCGGGTCGGACGTCGGTCAC–3'
ZDHHC12 sg2 Forward [CHOPCHOP Team, 2025]	5'-CACCGCGGGGCACCAGCTGGTGACG–3'
ZDHHC12 sg2 Reverse [CHOPCHOP Team, 2025]	5'-AAACGTCACCAGCTGGTGCCCGCG–3'
ZDHHC12 sg3 Forward [CHOPCHOP Team, 2025]	5'-CACCGTGAGTGTGCCCGCTGCAGG–3'
ZDHHC12 sg3 Reverse [CHOPCHOP Team, 2025]	5'-AAACCTGCAGCGGGCACACTCAC–3'
ZDHHC13 sg1 Forward [CHOPCHOP Team, 2025]	5'-CACCGGTGGACTGGCAGTGCATAG–3'
ZDHHC13 sg1 Reverse [CHOPCHOP Team, 2025]	5'-AAACCTATGCAGTGCAGTCCACCG–3'
ZDHHC13 sg2 Forward [CHOPCHOP Team, 2025]	5'-CACCGTGACTGGCGTGACGCCGTC–3'
ZDHHC13 sg2 Reverse [CHOPCHOP Team, 2025]	5'-AAACGACGGCGTCACGCCAGTCAC–3'
ZDHHC13 sg3 Forward [CHOPCHOP Team, 2025]	5'-CACCGTGATATCTAACAGGCCT–3'
ZDHHC13 sg3 Reverse [CHOPCHOP Team, 2025]	5'-AAACAGGCCTGTTAGATATCAC–3'

3.4 Metabolic Labeling and Click Chemistry

3.4.1 Cell Lysis and Membrane Fractionation

Following labeling, cells were washed twice with ice-cold PBS and lysed in lysis buffer containing 1 mM Phenylmethylsulfonyl fluoride (PMSF) (Cayman, Cat. No. 14333), and 1 mM hexadecylsulfonyl fluoride (HDSF; Santa Cruz Biotechnology, Cat. No. sc-221708), supplemented with protease inhibitors. Pellet was sonicated on ice for 3 cycles of 20 seconds each (70% amplitude, 50% power). Protein concentrations were measured using the BCA assay (Thermo Scientific), and equal amounts of protein were used for membrane pelleting. For comparisons based on SILAC, equal amounts of light and heavy lysates were mixed in a 1:1 ratio according to protein concentration. To enrich for membrane-associated proteins, the lysates were centrifuged at 100,000× g for 1 hour at 4°C using a 90-TI ultracentrifuge rotor. The membrane pellet was resuspended in 2% SDS in PBS.

3.4.2 Click Chemistry Reaction (CuAAC)

For detection and enrichment of palmitoylated proteins, click chemistry was performed using the copper(I)-catalyzed azide–alkyne cycloaddition (CuAAC) reaction. Lysates were adjusted to a final concentration of 2% SDS in PBS and incubated with the following reagents at final concentrations: 500 µM biotin-azide (Cayman Chemical, Cat. No. 13040.5), 1 mM tris(2-carboxyethyl)phosphine (TCEP; Apollo Scientific, Cat. No. BIT0122), 100 µM TBTA (Cayman Chemical, Cat. No. 18816), and 1 mM $CuSO_4$ (Lach-Ner).

TCEP was freshly prepared by dissolving in PBS to a concentration of 50 mM (14.35 mg/mL) and adjusted to pH 7.0 using 10 N KOH (∼0.5 µL per 300 µL). The TBTA ligand was prepared as a 50X stock by dissolving 8.85 mg of TBTA in 200 µL of a 20% DMSO and 80% *t*-butanol mixture. All components were added sequentially to the lysate, and the reaction was incubated for 1 hour at room temperature in the dark with gentle shaking.

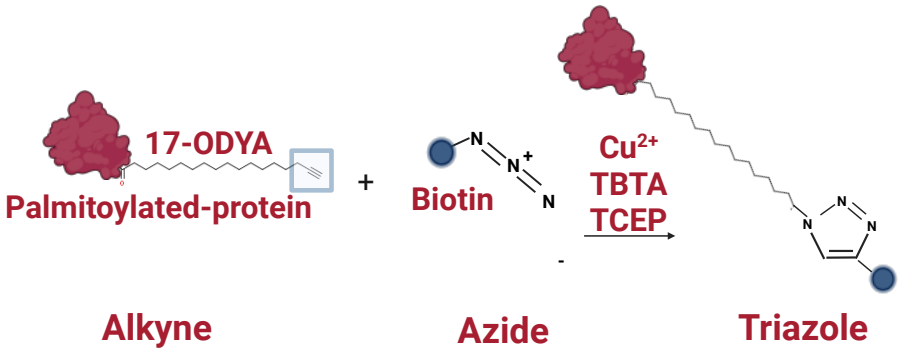

Figure 3.3: Enzymatic reaction of click chemistry (Created with BioRender.com).

3.4.3 Protein Precipitation and Sample Cleanup

To remove unreacted components following the CuAAC reaction, proteins were precipitated using the methanol–chloroform method. For each 1 mL of reaction volume, four volumes (4 mL) of ice-cold methanol were added and mixed thoroughly, followed by the addition of 1.5 volumes (1.5 mL) of chloroform under a fume hood. The mixture was vortexed again, and three volumes (3 mL) of deionized water were added, resulting in a cloudy appearance. Samples were centrifuged at 4,000 × g for 20 minutes at room temperature, forming a white protein layer at the interface between the aqueous and organic phases. The upper phase was carefully aspirated without disturbing the interface.

The precipitate was washed with 3 mL of cold methanol, vortexed, and centrifuged again at 4,000 × g for 10 minutes. This methanol wash was repeated once more. After the final centrifugation, residual methanol was removed and the pellet was processed for streptavidin-based enrichment as described in Section 3.5.

3.5 Streptavidin-Based Enrichment and Proteomic Sample Preparation

3.5.1 Streptavidin bead binding and washing

Following click chemistry-based biotin labeling, protein samples were solubilized in 6 M urea (Sigma-Aldrich, Cat. No. 33247) and 2% SDS in PBS to ensure complete denaturation and dissociation from membrane compartments. To minimize interference with bead binding, samples were subsequently diluted 20-fold with PBS containing 0.1% SDS, reducing the concentration of urea and detergent while maintaining protein solubility.

Streptavidin Plus UltraLink™ Resin (Thermo Fisher Scientific, Cat. No. 88817) were equilibrated in PBS and added to the diluted samples at a bead volume proportional to the estimated protein content. The mixture was incubated at room temperature for 90 minutes with gentle rotation to allow for efficient binding of biotinylated proteins to the streptavidin surface.

After binding, beads were washed extensively to remove non-specifically associated proteins and residual click reagents. The wash steps included ten sequential washes with 1 mL PBS, followed by a single wash with 2 M urea in PBS to eliminate remaining non-covalent interactions and denature residual contaminants.

3.5.2 Peptide Desalting and High-pH Reversed Phase Fractionation

Following on-bead digestion, peptide samples were first desalted using C18 reversed-phase solid-phase extraction columns (Sep-Pak, Waters). Columns were conditioned with 100% methanol, followed by 0.1% formic acid in water. Acidified peptide samples were loaded onto the columns, washed extensively with 0.1% formic acid to remove salts and other interfering substances, and eluted with 80% acetonitrile containing 0.1% formic acid. The eluates were dried under vacuum using a SpeedVac concentrator until high-pH fractionation.

High-pH reversed-phase fractionation was performed using a tip-based StageTip method with homemade microcolumns packed with five C18 disks per tip. Dried peptides were reconstituted in 50 µL of 15 mM ammonium hydroxide containing 2%

acetonitrile (pH 10), referred to as the loading buffer. Prior to peptide binding, StageTips were conditioned sequentially with 100 µL methanol, and two rounds of 100 µL 50% acetonitrile, each followed by centrifugation at 2500 × g.

Peptide samples were loaded onto the StageTips via centrifugation. Eighteen individual ammonium hydroxide buffers containing increasing concentrations of acetonitrile (2–90%) were freshly prepared on the day of use by mixing appropriate volumes of 1 M NaOH, acetonitrile, and distilled water. Each elution was performed in 100 µL volumes using the following acetonitrile percentages in 15 mM ammonium hydroxide: 2, 6, 10, 12, 14, 16, 18, 20, 22, 24, 26, 28, 30, 33, 36, 40, 60, and 90%. Flow-through from the loading step was collected as the first fraction (2% ACN). Eluates were dried immediately in a SpeedVac concentrator.

For LC-MS/MS analysis, each dried fraction was resuspended in 10 µL of MS loading buffer, vortexed, sonicated at 20% amplitude for 5 minutes, and centrifuged to remove particulates. To reduce the number of injections and optimize peptide coverage, fractions were recombined as follows:

- **FR1:** 2% and 90% ACN
- **FR2:** 6%, 16%, 24%, and 33% ACN
- **FR3:** 10%, 18%, 26%, and 36% ACN
- **FR4:** 12%, 20%, 28%, and 40% ACN
- **FR5:** 14%, 22%, 30%, and 60% ACN

3.6 LC-MS/MS Acquisition and Data Analysis

3.6.1 Mass Spectrometry Instrument Settings

Peptide mixtures obtained after on-bead digestion and high-pH fractionation were analyzed using a Thermo Scientific Orbitrap Exploris 480 mass spectrometer coupled to an EASY-nLC 1200 nano-flow UHPLC system. Peptides were reconstituted in 0.1% formic acid and loaded onto a C18 reverse-phase analytical column (75 μm

× 25 cm, packed with 2 μm C18 particles, 100 Å pore size). The column was maintained at 40°C, and peptides were eluted using a linear gradient of 5% to 35% acetonitrile in 0.1% formic acid over 90 minutes at a flow rate of 300 nL/min. The mass spectrometer was operated in data-dependent acquisition (DDA) mode. Full MS scans were acquired in the Orbitrap with a mass range of m/z 350–1,500 at a resolution of 60,000 (at m/z 200). The automatic gain control (AGC) target was set to 3×10^6 with a maximum injection time of 20 ms. The top 20 most intense precursor ions were selected for higher-energy collisional dissociation (HCD) fragmentation with a normalized collision energy (NCE) of 28%.

MS/MS spectra were acquired in the Orbitrap at a resolution of 15,000, with an AGC target of 1×10^5 and a maximum injection time of 50 ms. Dynamic exclusion was enabled for 30 seconds to avoid repeated sequencing of abundant peptides.

3.6.2 Identification of Palmitoylated Proteins via SAINT

To identify high-confidence palmitoylated proteins, mass spectrometry data obtained from 17-ODYA labelled samples and control samples treated with palmitic acid were analyzed using the SAINT (Significance Analysis of INTeractome) scoring algorithm implemented via SAINTexpress. Label-free quantification (LFQ) was first performed using FragPipe (v23.0) with the MSFragger search engine. Raw files were searched against the UniProt Homo sapiens reference proteome (UP000005640) using default parameters with the following settings: precursor and fragment mass tolerances set to ±20 ppm, up to two missed cleavages allowed, and trypsin/P as the digestion enzyme. Carbamidomethylation of cysteine was set as a fixed modification, while oxidation of methionine and N-terminal acetylation were set as variable modifications. The `IonQuant` module was used for LFQ with match-between-runs disabled.

Following peptide and protein inference, data were imported into `SAINTexpress`, where 17-ODYA samples were designated as the "experimental group" and palmitic acid-treated samples served as controls to account for nonspecific background binding. SAINT probability scores were used to classify proteins with high confidence, using a default threshold of SAINT score ≥ 0.7 and Bayesian FDR ≤ 0.05.

3.6.3 Quantitative SILAC Analysis with MaxQuant

To quantify dynamic changes in protein palmitoylation across cell cycle stages, Stable Isotope Labeling by Amino acids in Cell culture (SILAC) data were analyzed using MaxQuant (version 2.2.0.0). Raw LC-MS/MS data were processed using default parameters unless otherwise specified. Using the integrated Andromeda search engine, database searches were performed against the UniProt human reference proteome (UP000005640).

Carbamidomethylation of cysteine residues was set as a fixed modification, while oxidation of methionine and N-terminal acetylation were considered variable modifications. Isotopic labeling was defined as Lys8 (L-lysine labeled with heavy carbon and nitrogen atoms) and Arg10 (L-arginine labeled with heavy carbon and nitrogen atoms), which add +8 Da and +10 Da to the mass of the peptides, respectively. Tryptic peptides shorter than six amino acids were excluded, and up to two missed cleavages were allowed during digestion. To ensure more consistent peptide detection across biological replicates, the 'Match between runs' and 'Requantify' settings were used.

Protein quantification was performed using unique and razor peptides, requiring at least two ratio counts. For peptide identification, the mass tolerances were set to 20 ppm for the initial search and 7 ppm for the main search, with an MS/MS match tolerance of 0.5 Da. To ensure identification accuracy, both the peptide-spectrum match and protein false discovery rates (FDR) were controlled at 1% using a target-decoy approach. The resulting protein ratios (heavy/light) provided a quantitative readout of differential palmitoylation enrichment throughout interphase, mitosis, and cytokinesis.

3.7 Validation Experiments

3.7.1 Western Blot Analysis of Enriched Proteins

Following the completion of the metabolic labeling and click chemistry protocol, proteins pulldown by streptavidin-based enrichment. Specifically, after labeling

with either 17-ODYA or palmitic acid and subsequent Cu(I)-catalyzed azide-alkyne cycloaddition (CuAAC) reactions, biotin-tagged palmitoylated proteins were selectively captured using streptavidin resin. Excess unbound material was removed through extensive washing, and bound proteins were eluted using excess biotin.

To verify the successful enrichment of palmitoylated proteins and assess the modification status of specific candidates, eluted samples were separated by SDS-PAGE and transferred onto nitrocellulose membranes. Membranes were blocked in 1% BSA in TBST and probed with primary antibodies targeting proteins of interest (e.g., ZDHHC5). Detection was performed using host-specific HRP-conjugated secondary antibodies. Bands were visualized using chemiluminescence (ECL, Thermo Fisher Scientific) and quantified with ImageJ.

3.7.2 Immunofluorescence Imaging of Palmitoylation

To investigate the subcellular localization of palmitoylated proteins, immunofluorescence microscopy was performed on fixed cells following click chemistry labeling. Cells were first fixed with 4% paraformaldehyde (PFA) in PBS for 15 minutes at room temperature and permeabilized with 0.1% Triton X-100 in PBS for 5 minutes.

Click chemistry was then carried out on coverslips using a labeling mix containing 100 µM biotin-azide (Cayman Chemical, Cat. No. 13040.5), 1 mM $CuSO_4$, 1 mM freshly neutralized TCEP, and 100 µM TBTA ligand in PBS. The reaction was incubated for 1 hour at room temperature in the dark. Excess reagents were removed by extensive PBS washing. After three PBS washes, cells were blocked in 2% BSA for 1 hour at room temperature.

Biotin-labeled palmitoylated proteins were visualized using Streptavidin–Alexa Fluor 488 (Invitrogen, Cat. No. S32354; dilution 1:1000) in PBS containing 2% BSA. Nuclei were counterstained with DAPI (Sigma-Aldrich, D8417). Images were acquired using a Leica DMi8 widefield fluorescence microscope (LAS X Software) or a Leica DMi8/SP8 TCS-DLS confocal microscope, using consistent acquisition settings across all conditions.

3.7.3 Proximity Ligation Assay (PLA)

To examine the potential intracellular interactions between metabolically labeled palmitoylated proteins and specific target proteins, Proximity Ligation Assay (PLA) was performed using the Duolink® In Situ Red Starter Kit (Sigma-Aldrich, Cat. No. DUO92101) according to the manufacturer's protocol. HeLa Kyoto cells were seeded on sterile glass coverslips and synchronized according to experimental requirements. After synchronization, cells were fixed in 3.2% paraformaldehyde (PFA) for 15 minutes at room temperature and permeabilized using 0.1% Triton X-100 in PBS for 10 minutes.

Blocking was carried out using Duolink Blocking Solution for 30 minutes at 37 °C. Cells were then incubated overnight at 4 °C with pairs of primary antibodies to detect close proximity between biotin-labeled palmitoylated proteins and potential interactors. Two interaction pairs were evaluated:

1. Anti-biotin (rabbit, custom; 1:20,000) and anti-α-tubulin (mouse, Cell Signaling, Cat. No. 3873S; 1:1,000).

2. Anti-biotin (mouse, Santa Cruz, Cat. No. sc-101339; 1:100) and anti-Ezrin (rabbit, Cell Signaling, Cat. No. 3145S; 1:500).

Negative controls included samples incubated with only one of the primary antibodies to assess background signal. After primary antibody incubation, PLA probe hybridization was carried out at 37 °C for 1 hour, followed by ligation for 30 minutes and amplification for 100 minutes, according to the kit instructions. After final washes, slides were mounted with Duolink Mounting Medium containing DAPI and prepared for microscopic analysis.

PLA signals were detected as distinct red puncta, indicating proximity (<40 nm) between the antibody-labeled targets. Images were acquired using a fluorescence microscope, and the number and distribution of PLA signals were quantified using Fiji (ImageJ) software.

3.8 Live-Cell Imaging

3.8.1 Expression of LifeAct-GFP

To visualize actin cytoskeleton dynamics during cell division, HeLa Kyoto cells were transiently transfected with the LifeAct-GFP plasmid using Lipofectamine 3000 (Thermo Fisher Scientific, Cat. No. L3000008), according to the manufacturer's protocol. After 24 to 48 hours of transfection, GFP-positive cells were identified via fluorescence microscopy, and those with moderate expression levels were selected to avoid overexpression-induced artifacts. Transfection efficiency and expression uniformity were visually confirmed before proceeding to imaging.

3.8.2 Time-Lapse Microscopy Conditions

Time-lapse live-cell imaging was performed using a Leica DMi8 widefield fluorescence microscope (Leica Microsystems), equipped with a stage-top incubation chamber maintaining physiological conditions (37 °C, 5% CO_2, and humidified atmosphere). Cells were seeded on glass-bottom dishes and imaged using a 63× Plan Apo 1.4 NA oil-immersion objective. Images were acquired every 2 to 3 minutes for up to 12 hours to capture mitotic progression and cytokinesis dynamics. In most cases, a single focal plane was recorded; however, z-stacks were also acquired when necessary to assess three-dimensional cellular morphology.

3.8.3 Duration Analysis

Time-lapse image sequences were analyzed using FIJI/ImageJ software. The duration of specific mitotic stages was quantified by manually measuring the time intervals between characteristic cellular events, including rounding, metaphase alignment, anaphase onset, cleavage furrow ingression, and the completion of cytokinesis (Figure 4.38).

Phenotypic abnormalities, such as prolonged metaphase, failed cytokinesis, or the formation of multinucleated cells were documented and quantified. For each experimental condition, at least 50 mitotic cells were evaluated in three independent

biological replicates. Statistical analyzes and graphical representations of mitotic timing were performed using GraphPad Prism software.

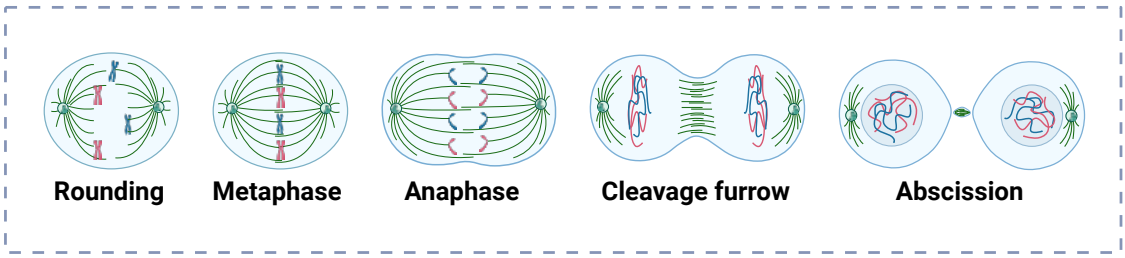

Figure 3.4: Quantification of Mitotic Progression (Created with BioRender.com).

Table 3.2: siRNA information including target genes, codes, amounts, and sequences.

siRNA	**Kod**		**Amount**	**Target Sequence**
Non Targeting	D-001810-10-05	ON-TARGETplus Non-targeting pool	5 nmol	
ZDHHC6	L-014101-00-0005	ON-TARGETplus SMARTpool (64429)	5 nmol	
	J-014101-05	ZDHHC56		GAAGGUGUUUCAAGAAUAA
	J-014101-06	ZDHHC56		CAAUACAGCUUAACAAUAG
	J-014101-07	ZDHHC56		CACCGAAGAGCCUCGAAUA
	J-014101-08	ZDHHC56		UCAGAAGUGUUCGCUAUAA
ZDHHC12	L-016296-01-0005	ON-TARGETplus SMARTpool ZDHHC12 (84885)	5 nmol	
	J-016296-09	ZDHHC12		GAAUCACGCUGGUGCUCUU
	J-016296-10	ZDHHC12		GCUUCAAGUCAGACAGAUC
	J-016296-11	ZDHHC12		GGGAAUUCAUCUCCUCACA
	J-016296-12	ZDHHC12		AAGCAAGUCCAGUCUUAAA
ZDHHC4	L-016699-01-0005	ON-TARGETplus SMARTpool ZDHHC4 (55146)	5 nmol	
	J-016699-09	ZDHHC4		GAGCUGUAGUUCCCGUUUA
	J-016699-10	ZDHHC4		CGGAGCAACCUUCAAGAGA
	J-016699-11	ZDHHC4		AGACUACUAACGAGUGGUA
	J-016699-12	ZDHHC4		AUUUAUACCAGGAGACUUA
ZDHHC2	L-020510-01-0005	ON-TARGETplus SMARTpool ZDHHC2 (51201)	5 nmol	
	J-018402-05	ZDHHC2		GACAGAUGCCAACUUAUAA
	J-018402-06	ZDHHC2		CCAAGGAUCUUCCCAUCUA
	J-018402-07	ZDHHC2		ACAAAUGGCCUACCUGAUA
	J-018402-08	ZDHHC2		GGCAACAGAUUUACAGUAU
ZDHHC13	L-020510-01-0005	ON-TARGETplus SMARTpool ZDHHC13 (54503)	5 nmol	
	J-020510-09	ZDHHC13		GGUUCUUGGUUGGGUAUAA
	J-020510-10	ZDHHC13		GUAUGUGGCUGGAUUAUAU
	J-020510-11	ZDHHC13		GGACAUCACAGUACACCAU
	J-020510-12	ZDHHC13		GGGCUAUUGGAUACAUAUU
ZDHHC24	L-026601-01-0005	ON-TARGETplus SMARTpool ZDHHC24 (254359)	5 nmol	
	J-026601-09	ZDHHC24		UCAGUAAGGAAGUCGGGUU
	J-026601-10	ZDHHC24		UGCUCAACCUGCUGGGCAA
	J-026601-11	ZDHHC24		GGGCUUGGGCCGUGACUUA
	J-026601-12	ZDHHC24		GUUAAUAAAGCACUGACUU

Chapter 4

RESULTS

4.1 Interphase and Mitotic Cells Have Different Palmitoylation Profiles

Palmitoylation, a reversible lipid based PTM, is an important modulator of the regulating protein localization, stability, and interaction dynamics. Cell division may be regulated by palmitoylation since palmitic acid attachment to the proteins influences their membrane binding affinities and function and localization. Its role in cell division has not been well characterized yet despite its established roles in various biological roles. Palmitoylation profiles were examined in interphase and mitosis sycnhronized cells respectively to investigate whether it plays a role in cell division (Figure 4.1). Interphase synchronization was achieved using a double thymidine block, while mitotic arrest at prometaphase was induced by STLC treatment. Cells were incubated overnight with 17-ODYA, an alkyne-functionalized palmitic acid analog, to metabolically label palmitoylated proteins. As a control, a separate set of cells was incubated under identical conditions with palmitic acid, which lacks the terminal alkyne group required for the click chemistry reaction. These control samples were processed in parallel and used to define a background proteome to identify and filtering out nonspecific protein interactions during downstream statistical analysis. Following cell harvesting, PMSF and HDSF, serine-specific protease inhibitors, along with a protease inhibitor cocktail were directly added to the cells to preserve palmitoylation.The proteins were then subjected to membrane enrichment to eliminate cytosolic contaminants. Newly synthesized, 17-ODYA-labeled palmitoylated proteins were biotinylated via a copper-catalyzed click chemistry reaction (Cu^{2+}). Biotinylated proteins were subsequently enriched using streptavidin based pulldown. Following enrichment, proteins underwent reduction, alkylation,

and on-bead trypsin digestion. Peptides were then desalted using C18 StageTips and fractionated into 18 fractions using high pH reversed-phase chromatography and combined into 5 final fractions before being subjected to LC-MS/MS analysis. Raw data were processed in FragPipe, and identified proteins were further analyzed using SAINT.

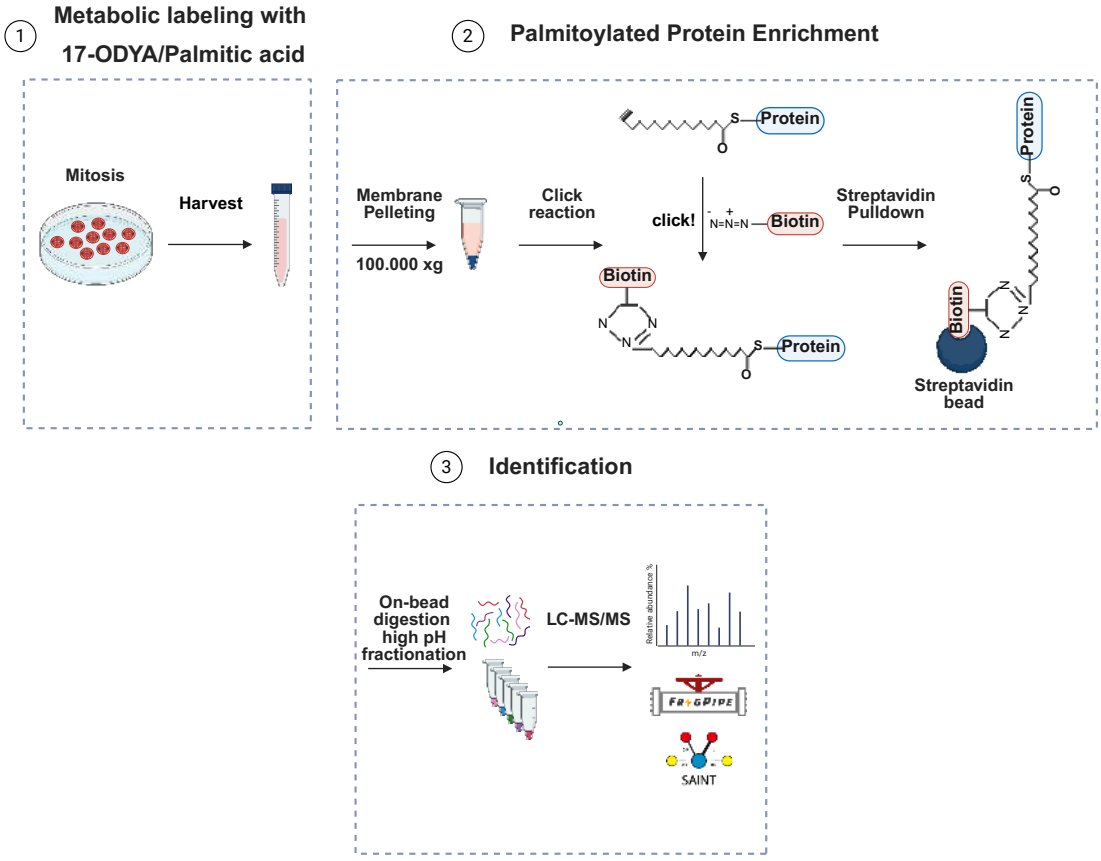

Figure 4.1: Workflow for metabolic labeling, enrichment, and identification of palmitoylated proteins using 17-ODYA and LC-MS/MS. (Created with BioRender.com)

Cells were incubated overnight with 17-ODYA or palmitic acid (Palm) as a negative control, followed by click chemistry-based biotinylation. Biotinylated proteins were visualized by streptavidin blotting. phospho-Histone H3 (phosH3) ,mitotic marker, was used to confirm mitotic synchornization efficiency (Figure 4.2). In palmitic acid labelled cells, only two prominent bands corresponding to endogenously

biotinylated proteins were detected, shows minimal background signal. 17-ODYA labelled cells showed prominent biotin labeling, especially in interphase condition.The efficiency of synchronization was validated by probing for phosH3, a mitotic marker, which was strongly detected under mitotic conditions (Figure 4.2). These results confirm the specificity of 17-ODYA–mediated labeling and indicate dynamic palmitoylation regulation during the cell cycle.

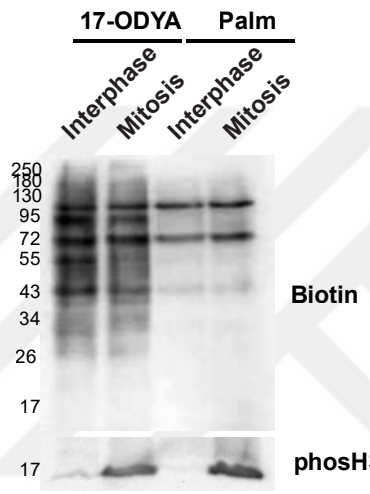

Figure 4.2: Representative streptavidin-HRP blot showing the labeling of palmitoylated proteins with 17-ODYA in interphase and mitotic cells.

A high correlation of protein intensities across biological replicates was observed. The enrichment and quantification workflow was highly reproducible for both samples labelled with palmitic acid and samples labelled with 17-ODYA, as indicated by the range of Pearson correlation coefficients from 0.87 to 0.94 (Figure 4.3). Consistent with this, principal component analysis (PCA) illustrated a separation between 17-ODYA and palmitic acid labelled samples along PC1 and PC2 (Figure 4.4).

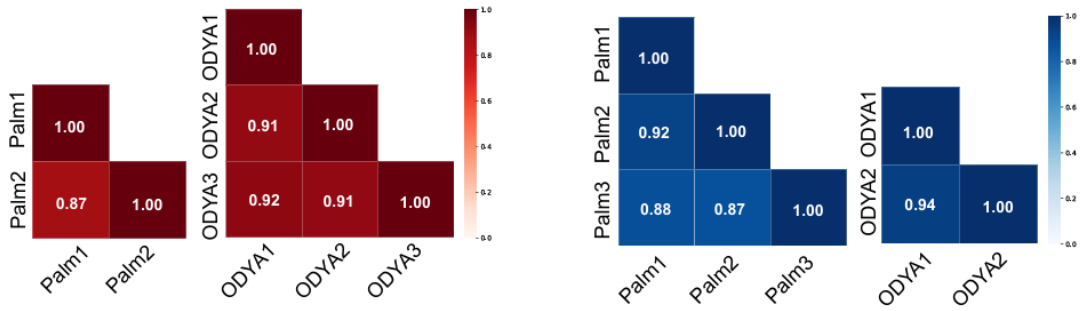

Figure 4.3: Pearson correlation heatmaps showing reproducibility across biological replicates. Blue and red color represent interphase and mitosis samples respectively.

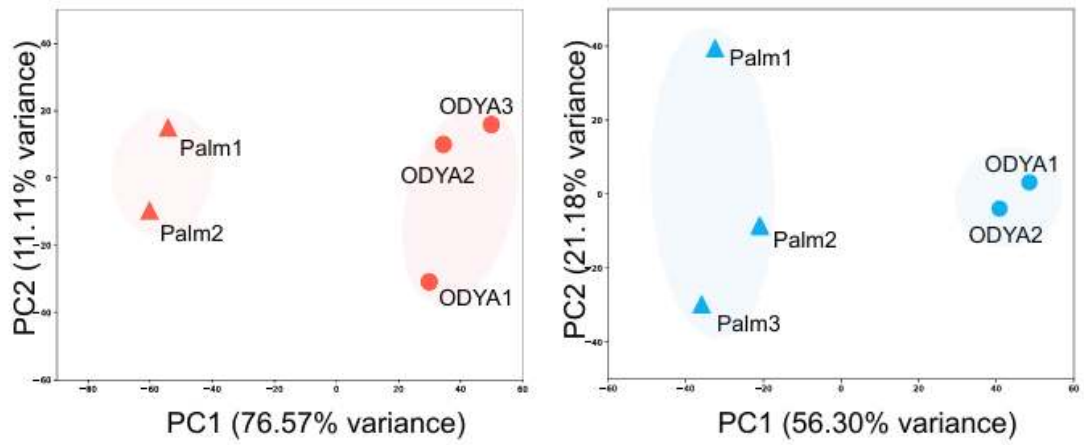

Figure 4.4: Principal component analysis (PCA) of palmitic acid– and 17-ODYA labelled samples.Blue and red color represent interphase and mitosis samples respectively.

The distribution of spectral count (SPC) values for quantified proteins indicates the overall abundance profile. 17-ODYA labelled mitosis and interphase cells have higher SPC values than palmitic acid labelled in both mitotic (Figure 4.5a) and interphase (Figure 4.5b) conditions, which is a proof of efficient labelling strategy. In both phases, samples labelled with 17-ODYA consistently showed higher intensities

than samples labelled with palmitic acid, according to the distribution of protein intensities. The higher efficiency of the 17-ODYA labelling method in enriching palmitoylated proteins is supported by these results. In both phases, samples labelled with 17-ODYA consistently showed higher intensities than samples labelled with palmitic acid, according to the distribution of protein intensities (Figure 4.6). The higher efficiency of the 17-ODYA labelling method to enrich palmitoylated proteins is further supported by these results.

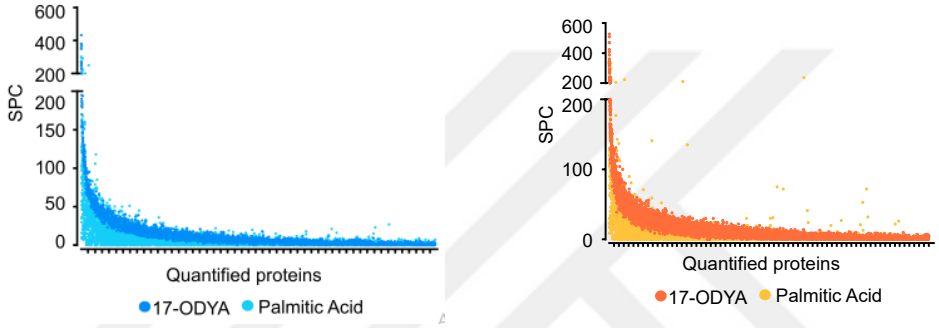

(a) Interphase synchronized (b) Mitosis synchronized

Figure 4.5: Comparison of spectral count (SPC) distributions.

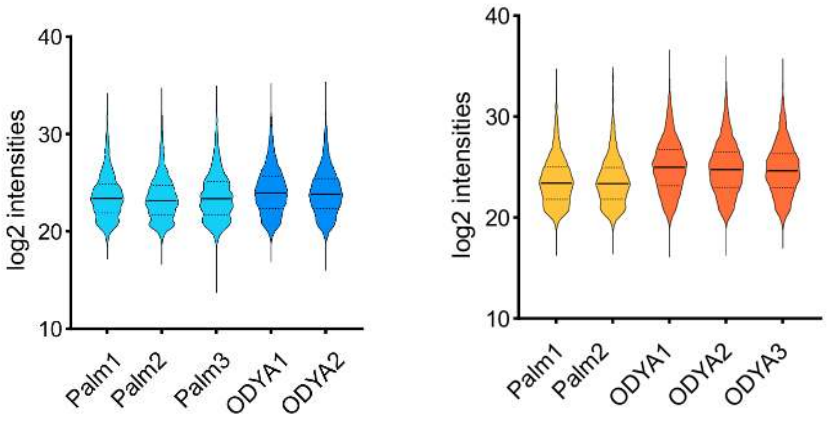

(a) Interphase synchronized (b) Mitosis synchronized

Figure 4.6: Comparison of protein intensity distributions across two independent metabolic labeling experiments.

SAINT was used to identify high-confidence palmitoylated proteins by analyzing raw mass spectrometry data, with palmitic acid labelled negative controls providing the statistical background. As a result of all the analyzes, 2,610 and 1,756 significant palmitoylated proteins were identified in mitotic and interphase samples, respectively, using SAINT analysis with a SAINT score of 0.7 and a BFDR score of 0.05 (Table 4.1). This analysis allowed for the identification of 5,077 proteins in the interphase sample and 6,604 proteins in the mitotic samples. CANX, TFRC, MYOF, and EGFR, which are well-known palmitoylated proteins, were identified in both samples, and they can be accepted as positive protein indicators in the datasets. Interestingly, multiple proteins of the DHHC family (ZDHHC5, ZDHHC6, ZDHHC13, and ZDHHC20) were also significant in the SAINT analysis, suggesting autopalmitoylation of PAT enzymes. When the SPC values were compared between interphase and mitotic conditions for MYOF, CANX, KIF11, PCDH1, INCENP, PCDH7, CCNB1, BUB1, and NUSAP1, dynamic palmitoylation during cell division can be suggested. The SPCs of these mitotic regulators, such as KIF11, INCENP, PCDH7, CCNB1, BUB1, and NUSAP1, were higher in mitotic samples than in interphase with SAINT scores above 0.8 and Bayesian FDR values below 0.02. According to this pattern, palmitoylation might be upregulated in a stage-specific way during mitosis.

Table 4.1: Comparison of protein palmitoylation levels in interphase and mitosis

Gene Name	**Interphase**			**Mitosis**			**Number of palmitoyl-proteome studies**
	ODYA	Palm	Saint Score	ODYA	Palm	Saint Score	
CANX	117 | 127	26 | 20 | 11	1	203 | 190 | 200	20 | 23	1	18 of 22
TFRC	254 | 269	36 | 35 | 10	1	362 | 334 | 343	23 | 30	1	17 of 22
MYOF	262 | 232	16 | 30 | 9	1	318 | 332 | 339	9 | 17	1	9 of 22
ZDHHC5	61 | 57	0 | 0 | 0	1	35 | 43 | 42	0 | 0	1	9 of 22
ZDHHC13	5 | 2	0 | 0 | 0	0.99	9 | 5 | 8	0 | 0	1	8 of 22
ZDHHC6	9 | 12	0 | 0 | 0	1	5 | 8 | 9	0 | 0	1	8 of 22
CLCC1	24 | 21	2 | 5 | 0	1	22 | 26 | 31	0 | 1	1	7 of 22
ZDHHC20	8 | 9	0 | 0 | 0	1	12 | 16 | 15	0 | 0	1	7 of 22
CAPZB	8 | 4	0 | 1 | 1	0.98	9 | 11 | 10	1 | 3	1	5 of 22
EZR	8 | 9	1 | 3 | 2	0.98	-	-	-	5 of 22
CCDC47	-	-	-	19 | 16 | 18	1 | 4	1	4 of 22
EGFR	57 | 55	12 | 13 | 4	1	50 | 65 | 54	9 | 8	1	4 of 22
TUBB3	-	-	-	8 | 8 | 6	3 | 2	0.85	4 of 22
CCDC51	20 | 17	2 | 3 | 1	1	29 | 28 | 28	1 | 4	1	3 of 22
KIF11	18 | 24	10 | 6 | 4	0.86	81 | 93 | 61	11 | 11	1	3 of 22
PCDH1	8 | 8	0 | 0 | 0	1	8 | 9 | 11	0 | 0	1	3 of 22
RAB3GAP2	23 | 29	11 | 5 | 4	0.99	58 | 63 | 51	8 | 11	1	3 of 22
TUBA1C	-	-	-	4 | 4 | 8	1 | 1	0.96	3 of 22
ANAPC1	11 | 5	2 | 1 | 1	0.95	-	-	-	2 of 22
ANAPC7	-	-	-	19 | 28 | 19	8 | 3	0.98	2 of 22
AURKB	13 | 11	3 | 4 | 0	0.99	-	-	-	2 of 22
INCENP	12 | 13	4 | 7 | 1	0.8	40 | 33 | 35	9 | 5	1	2 of 22
KIF14	-	-	-	70 | 73 | 70	21 | 13	1	2 of 22
PCDH7	23 | 24	0 | 0 | 0	1	22 | 24 | 32	0 | 0	1	2 of 22
PLK1	8 | 5	1 | 2 | 2	0.88	-	-	-	2 of 22
ZDHHC7	9 | 8	0 | 0 | 0	1	10 | 8 | 8	0 | 0	1	2 of 22
ANAPC5	2 | 3	0 | 0 | 0	0.99	5 | 4 | 5	1 | 1	0.97	1 of 22
ANLN	12 | 17	5 | 5 | 4	0.8	49 | 46 | 44	14 | 8	1	1 of 22
CCDC86	-	-	-	16 | 10 | 5	0 | 0	1	1 of 22
CCNB1	3 | 4	0 | 0 | 1	0.99	27 | 24 | 21	3 | 0	1	1 of 22
CENPC	3 | 2	0 | 0 | 0	0.99	4 | 6 | 6	0 | 0	1	1 of 22
MTOR	13 | 13	5 | 4 | 5	0.84	40 | 56 | 29	8 | 8	1	1 of 22
TUBGCP2	8 | 12	3 | 3 | 1	0.97	33 | 38 | 25	1 | 1	1	1 of 22
BUB1	4 | 3	0 | 0 | 1	0.99	29 | 27 | 25	3 | 2	1	0 of 22
CCNB2	-	-	-	16 | 11 | 13	3 | 2	1	0 of 22
NUSAP1	-	-	-	28 | 22 | 27	6 | 6	1	0 of 22

To evaluate the biological relevance of the palmitoylated proteome, identified

proteins were cross-referenced with the SwissPalm database. In mitotic samples, 1,650 proteins (63.2%) were previously annotated as palmitoylated in palmitoyl-proteome datasets, including 131 with experimental validation, while 829 proteins (31.8%) had no prior annotation. In interphase samples, 1,252 significant proteins (71.3%) had palmitoylation-related annotations, including 116 proteins (6.6%) with experimental evidence, whereas 388 proteins (22.1%) lacked any prior annotation (Figure 4.7). Notably, the annotation rate observed for interphase-enriched proteins was substantially higher than the 25.8% background frequency reported for the full SwissPalm *H. sapiens* dataset, supporting the specificity of the enrichment approach.

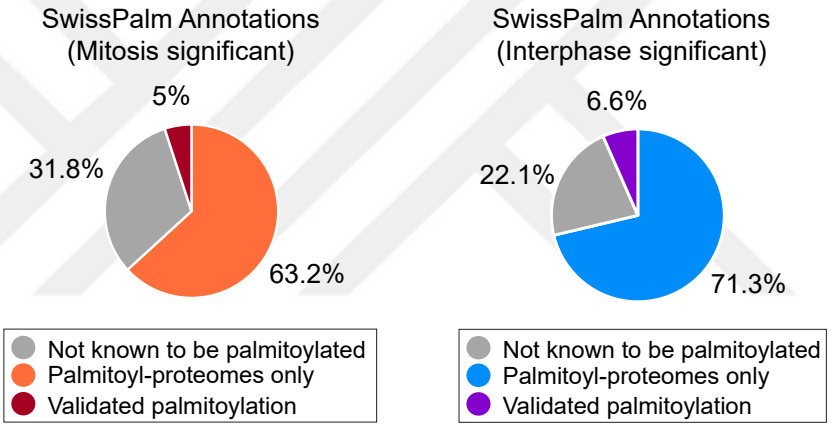

Figure 4.7: SwissPalm annotations of proteins significantly enriched during interphase (Blue) and mitosis (Red)

To validate selected palmitoylation candidates, Anillin and Cyclin B1 were each previously annotated in only one of 22 palmitoyl proteome studies in the SwissPalm database and BubR1, which had no prior annotation, were chosen for further analysis. All three proteins were identified as significant hits in the SAINT analysis. Western blot of mitotic samples labeled with 17-ODYA and palmitic acid confirmed the enrichment of these proteins under the 17-ODYA labeling condition, while no detectable signal was observed in palmitic acid controls. These findings support the selective palmitoylation of Anillin, BubR1, and Cyclin B1 (Figure 4.8).

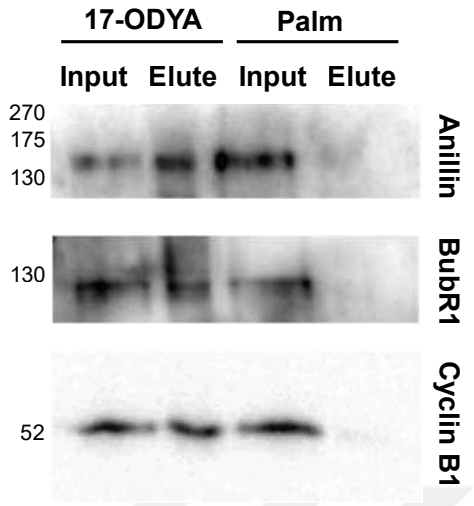

Figure 4.8: Western blot analysis of Anillin, BubR1, and Cyclin B1 in input and eluted fractions from 17-ODYA and palmitic acid treated mitotic samples.

Functional enrichment analysis using g:Profiler was performed on significant proteins from mitotic and interphase datasets to identify phase-specific functions. Representative Gene Ontology (GO) terms from significantly enriched categories were visualized to compare shared and distinct biological functions between phases (Figure 4.9). Interphase-enriched proteins were more strongly linked to cell adhesion, whereas mitosis-specific palmitoylated proteins were mainly linked to vesicular transport and cell division-related processes. According to this model, palmitoylation contributes to phase-specific functional programs by being temporally regulated throughout the cell cycle.

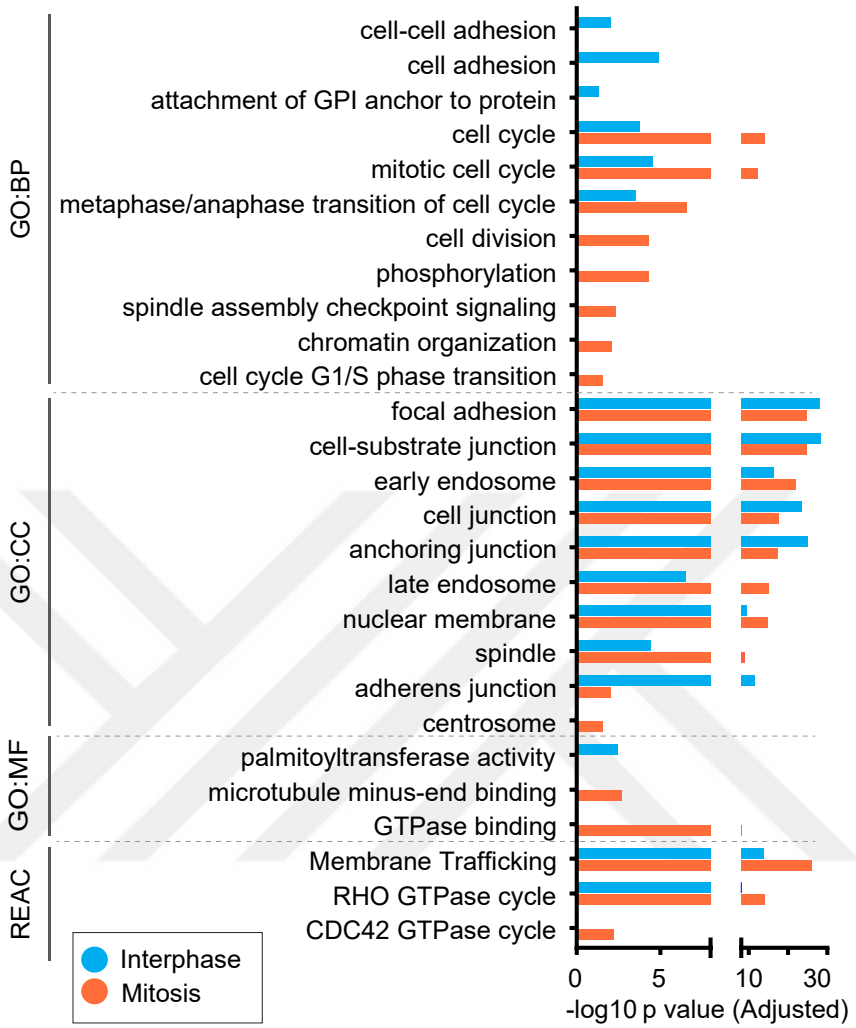

Figure 4.9: Functional enrichment analysis of palmitoylated proteins significantly enriched in interphase and mitosis. Top terms from Gene Ontology (GO:BP, GO:CC, GO:MF) and Reactome (REAC) are shown, ranked by adjusted p-values.

4.2 Cell Cycle Proteins are Selectively Palmitoylated Between Interphase and Mitosis

Although SAINT analysis previously indicated differential palmitoylation between interphase and mitosis, precisely assessing phase-specific patterns required a global and comparative quantification. A SILAC-based metabolic labelling approach was used combined with click chemistry–mediated enrichment to obtain quantitative

evaluation of palmitoylation dynamics in cell cycle stages. Heavy or light amino acids were used to differentially label HeLa cells for this purpose, and they were then synchronized to either the mitotic or interphase stages, respectively. A double thymidine block was used to achieve interphase synchronization, while STLC, an inhibitor of kinesin-5, was used to arrest mitotic cells. Using 17-ODYA, a palmitate analogue that integrates into freshly synthesized palmitoylated proteins, metabolic labelling was performed. Equal parts of the interphase and mitotic samples were combined in a 1:1 ratio after cell lysis, and membrane fractions were enriched. Click chemistry was then used to tag 17-ODYA-labeled proteins specifically using azide-conjugated biotin. Biotinylated proteins were separated under high pH conditions, digested on-bead with trypsin, enriched using streptavidin pulldown, and then analyzed using high-resolution LC-MS / MS (Figure 4.10). An identical parallel SILAC-labelled sample was prepared and processed up to the membrane enrichment step to account for potential differences in baseline protein abundance between interphase and mitotic conditions.

The efficiency of labeling and the depth of proteome coverage were evaluated by comparing LC-MS/MS data from light- and heavy-labeled samples. In the light-labeled condition, 4,278 proteins, 18,592 peptides, and 21,920 PSMs were identified and heavy-labeled samples showed comparable results, with 4,324 proteins, 21,142 peptides, and 25,916 PSMs detected. These findings (Table 4.2) indicate that SILAC labeling worked efficiently and provided a solid basis for quantitative proteomics.

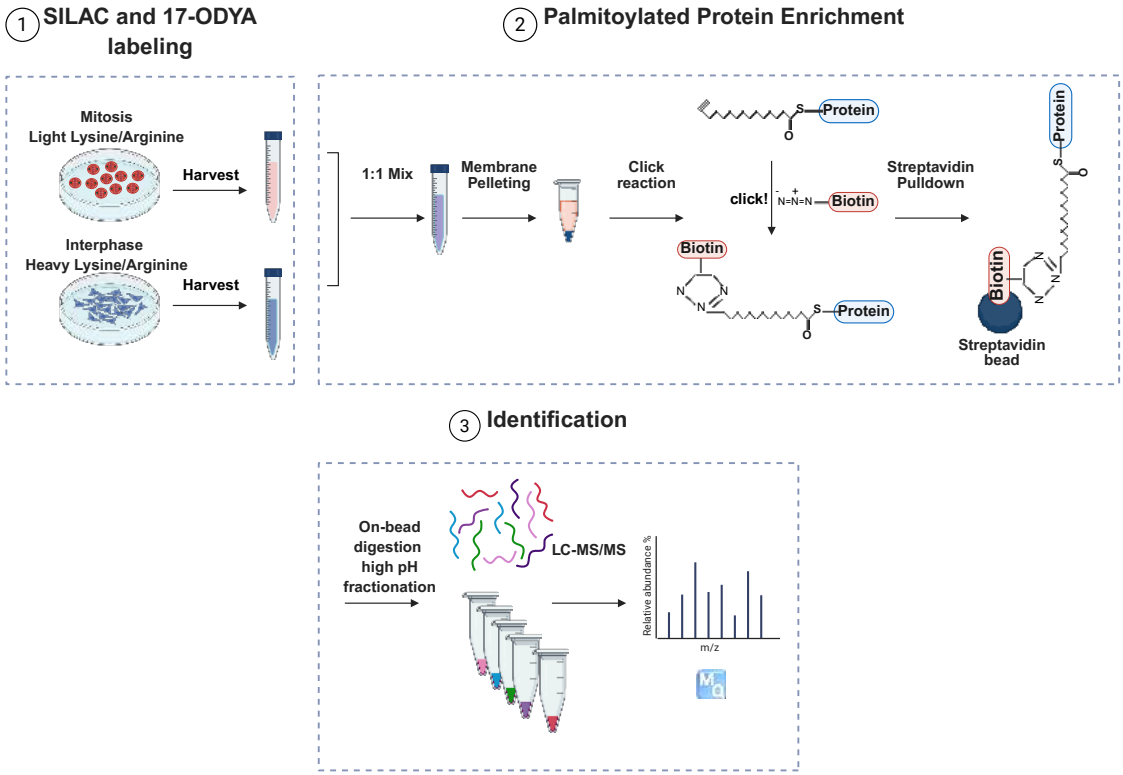

Figure 4.10: Workflow for SILAC-based metabolic labeling, enrichment, and identification of palmitoylated proteins using 17-ODYA labeling and LC-MS/MS analysis (Created with BioRender.com).

Table 4.2: Quantitative summary of SILAC-labeled samples.

	SILAC Light	**SILAC Heavy**
Signal	2.22E10	1.96E10
Proteins	4278	4324
Peptides	18592	21142
PSMs	21920	25916

The raw MS files were processed in MaxQuant, and the corresponding heavy-to-light (H/L) intensity of the 17-ODYA–labelled SILAC dataset (Figure 4.11) were normalized to the heavy-to-light (H/L) intensity ratios of the membrane-enriched

reference samples. Rather than relying on absolute intensities alone, this approach allowed us to evaluate the ratio of "palmitoylation to total protein" for each protein—essentially measuring palmitoylation occupancy. This was especially important for distinguishing whether an observed increase in signal was due to more palmitoylation or simply more of the protein itself.

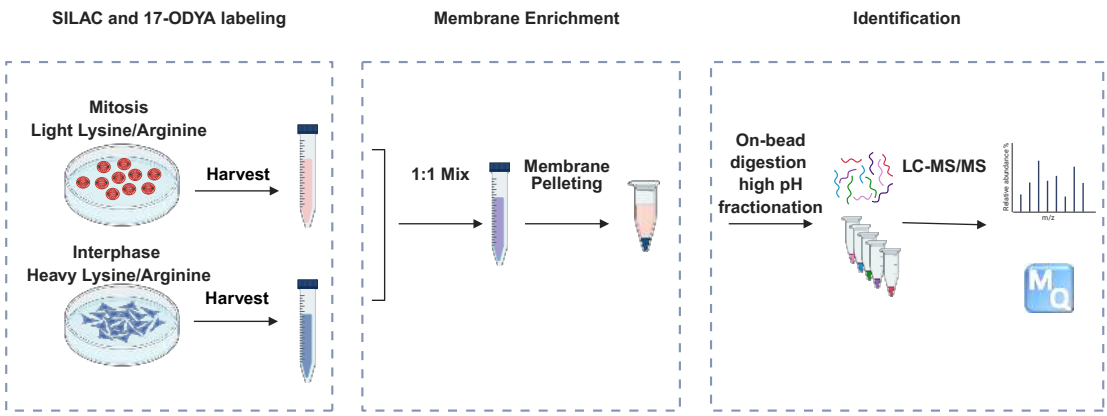

Figure 4.11: SILAC-based workflow for membrane proteome preparation used as a reference for normalization (Created with BioRender.com).

In the first panel (Figure 4.12), raw 17-ODYA signal intensities are shown for three biological replicates (BR1–BR3) in both mitotic (Light) and interphase (Heavy) samples. The signal ranges are similar across all replicates, showing that the experiments were consistent.

The second panel (Figure 4.12) shows the average protein abundance from membrane-enriched (ME) proteome data. This dataset was used as a reference for normalization. A major imbalance was not detected in the membrane-enriched profile, indicating that the data serve as a reliable reference for normalization.

In the third panel (Figure 4.12), median centering was used to normalize the 17-ODYA signal intensities. In other words, the median value of each sample was set to zero. The interphase and mitotic sample distributions stabilized and aligned after normalization. There was less variation between replicates, and the outcomes were more reliable. These enhancements demonstrate that the data can now be used to compare palmitoylation levels across conditions with greater accuracy and

dependability.

The fourth panel (Figure 4.12) shows normalized mitosis-to-interphase ratios for each biological replicate. The distributions are symmetric and closely aligned across replicates. This shows that technical noise has been successfully reduced. As a result, any remaining differences are more likely to reflect real biological changes, not experimental variation.

Together, this set of plots demonstrates both the high quality of the 17-ODYA enrichment data and the value of normalization in improving statistical reliability. The observed changes in palmitoylation indicate regulatory modulation that occurs independently of total protein expression levels.

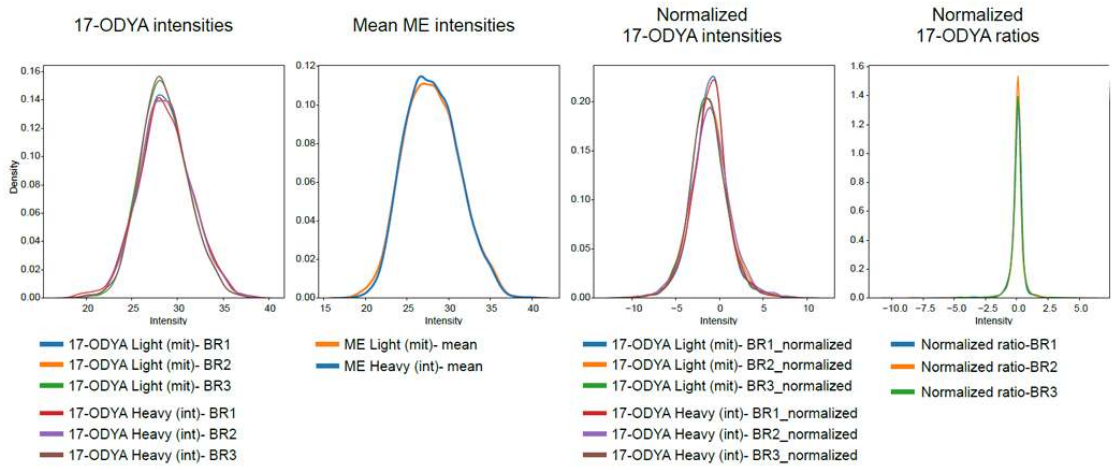

Figure 4.12: Density distributions of 17-ODYA–labeled peptides before and after normalization across biological replicates. A–B: Raw intensities; C: Normalized intensities; D: Normalized ratios.

As a result of the integrated click-chemistry and SILAC-based quantitative proteomics workflow, a total of 3,239 proteins were quantified with high confidence. Among these, 741 proteins (23%) exhibited significantly differential palmitoylation between interphase and mitosis, with 381 showing mitosis-selective and 360 interphase-selective palmitoylation patterns (Figure 4.13). These results point to a dynamic regulation of palmitoylation across the cell cycle and underscore the value

of quantitative proteomics in resolving stage-specific PTMs. Among the 741 significant proteins identified, 738 were found in the SwissPalm database. Of these, 474 proteins (64%) had previously been reported in palmitoyl-proteome studies, 28 (4%) had experimental validation, and 235 (32%) and 235 (32%) were not previously annotated. This distribution indicates that many identified proteins are supported by existing palmitoylation data, validating the reliability.

The same workflow was used to process SILAC-labelled cells treated with palmitic acid in parallel to confirm the specificity of the enrichment strategy. The palmitic acid-labelled dataset showed no significantly regulated proteins after normalization with total protein abundances, confirming the robustness and selectivity of the 17-ODYA–based quantification method.

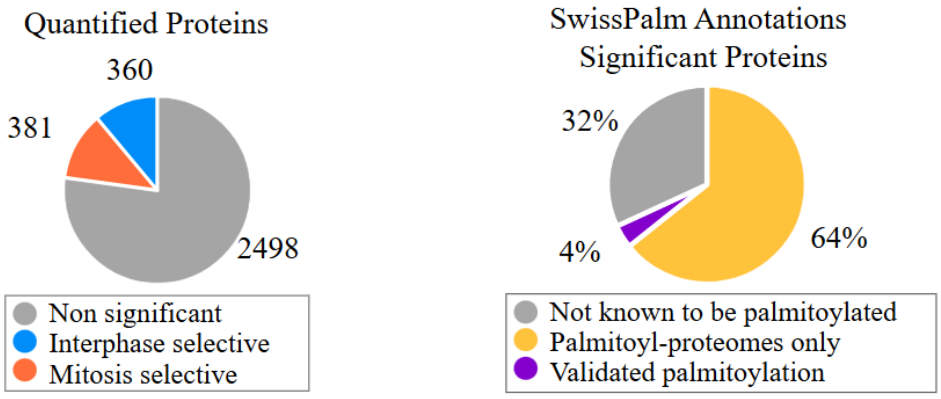

Figure 4.13: (a) Distribution of quantified proteins by statistical significance. (b) SwissPalm annotation status of significant proteins.

Differential palmitoylation during the cell cycle was analysed and showed that a number of cell cycle related proteins exhibit phase-selective patterns of modification. Mitotic and interphase samples exhibited different palmitoylation profiles, such that a subset of proteins was selectively enriched during mitosis (left, red), whereas others showed preferential palmitoylation during interphase (right, blue) (Figure 4.14). These findings imply that palmitoylation is dynamically controlled on a cell cycle-dependent manner and potentially offers a mechanism for functional modification of key regulatory proteins throughout mitotic progression or interphase maintenance.

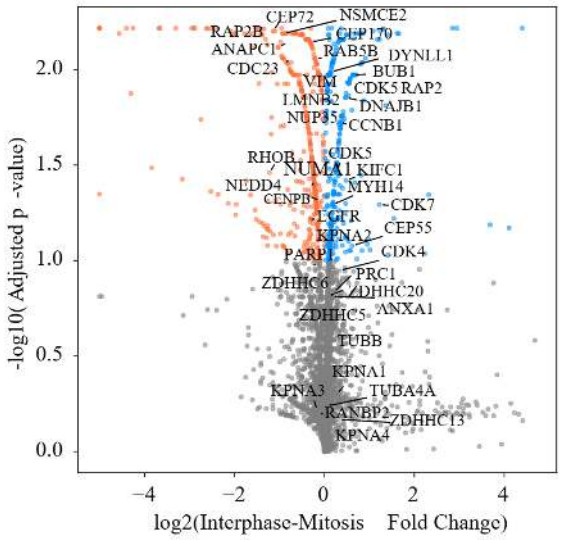

Figure 4.14: Volcano plot showing differentially palmitoylated proteins between interphase and mitosis.

To confirm phase-specific changes in palmitoylation, membrane fractions were collected from cells synchronized in interphase and mitosis. These proteins were labeled with 17-ODYA, biotinylated using click chemistry, and enriched with streptavidin beads. The enriched samples were then analyzed by Western blot. Antibodies against CEP55 and Cyclin B1 were used. Both proteins were present at similar levels in the total membrane fractions (Input). However, their levels in the palmitoylated fraction (Eluate) were different (Figure 4-15). CEP55 palmitoylation is enriched in mitosis. Cyclin B1 was also enriched in mitosis, but its signal was weak or absent in interphase. These results support the LC-MS/MS data and confirm that palmitoylation is regulated depending on the cell cycle phase for some proteins.

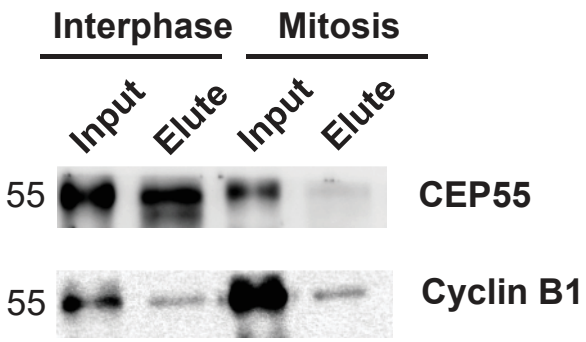

Figure 4.15: Western blot analysis showing palmitoylation levels of CEP55 and Cyclin B1 in interphase and mitotic cells.

GO term and pathway enrichment analyses were performed on the significantly enriched proteins to elucidate the functional significance of phase-specific palmitoylation further. Palmitoylation selective for interphase and mitosis has been associated with different biological processes (Figure 4.16), suggesting that functional roles are temporally regulated.

Cell adhesion and cytoskeletal organization terms, such as focal adhesion, cell-substrate junction, and actin filament binding, appeared to be highly overrepresented within the interphase-enriched dataset. In addition, the molecular function categories, cadherin binding and cell adhesion molecule binding, which came up enriched, imply that palmitoylation during interphase might function to sustain intercellular contacts and structural integrity. Additionally, the role of palmitoylation in mitotic progression has been shown by the enrichment of pathways, including SUMOylation of RNA-binding proteins and M-phase processes, including anaphase.

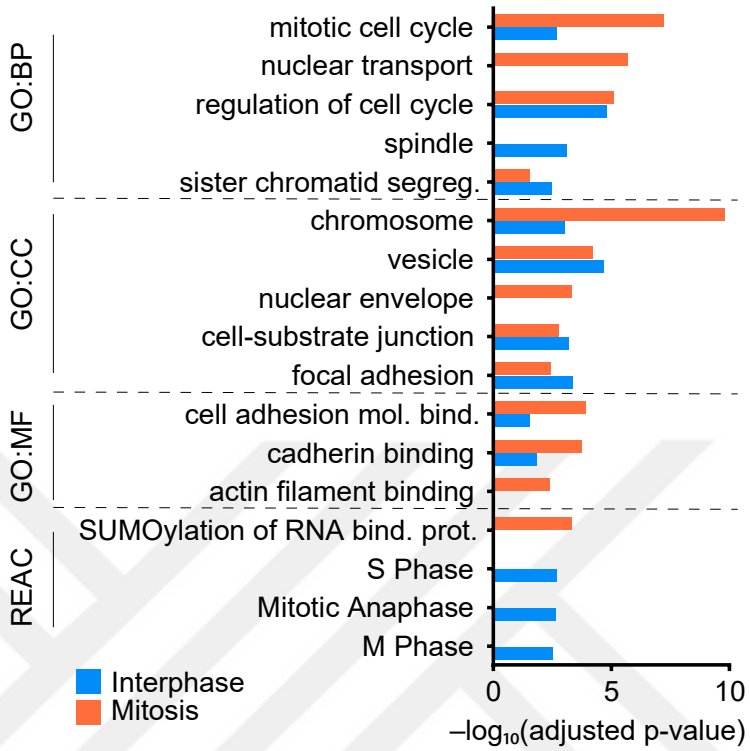

Figure 4.16: Enriched GO and Reactome terms for selectively palmitoylated proteins in interphase (blue) and mitosis (orange), ranked by $-\log_{10}$(adjusted p-value).

Term enrichment of all regulated proteins was performed to detail the palmitoylation dynamics of specific biological processes. The cell cycle was found to be the most significantly overrepresented category among the enriched terms. Proteins that are related to relevant GO terms cell division (GO:0051301) were mapped to show phase-specific palmitoylation profiles within these terms (Figure 4.17).

Cortical, midbody, and cleavage furrow-focused proteins uncovered mitosis preferential palmitoylation (orange)(Figure 4.17). Proteins that were localized to spindle, prometaphase, and centrosome spots, on the other hand, exhibited interphase enrichment (blue)(Figure 4.17). Indeed, anaphase-promoting complex components and anaphase-related proteins were preferentially palmitoylated during mitosis and imply functions during abscission and remodelling during late mitosis.

All these results exhibit a functionally different palmitoylation profile through-

out the cell cycle, such that mitotic palmitoylation is related to key cell division regulation events, and interphase palmitoylation biases towards adhesion and steric stability.

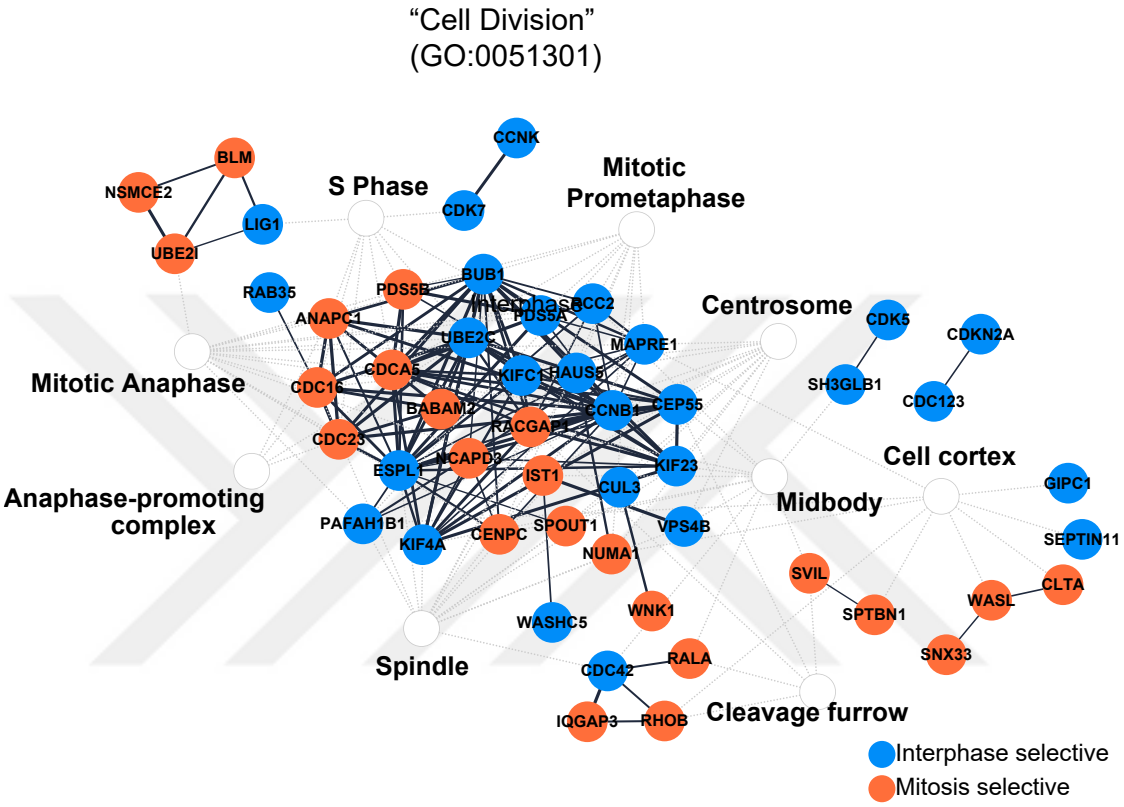

Figure 4.17: Figure 4.17: Protein interaction map of cell division–related palmitoylated proteins. Blue nodes are enriched in interphase, and orange nodes are enriched in mitosis.

4.3 Quantitative Comparison of Palmitoylation Dynamics and Their Co-clustering with the Phosphoproteome During Cell Division

To profile the dynamics of protein palmitoylation throughout the late stages of cell division, the palmitoyl-proteomes of cells undergoing mitosis and cytokinesis were quantitatively compared. HeLa cells metabolically labelled with light or heavy isotopes were synchronized in mitosis by treatment with 40 ng/L nocodazole. After 1.5 hours of release, cells progressing through bipolar cytokinesis were harvested.

Following 17-ODYA labelling, equal amounts of mitotic and cytokinetic samples were pooled and subjected to click chemistry, streptavidin-based enrichment, and on-bead tryptic digestion. After high-pH reversed-phase fractionation, peptides were analysed by LC-MS/MS (Figure 4.18). A parallel dataset generated from samples without 17-ODYA labelling and click chemistry was used to normalize the protein intensities and correct for underlying abundance differences Normalized heavy to light intensity ratios were found to be highly consistent within biological replicates, sharing more than 93% similarity, with cross-replicate similarity ranging between 73–85% (Figure 4.19). The specificity of the 17-ODYA labelling was highlighted by the fact that none of the significantly enriched proteins overlapped with those in the palmitic acid control group.

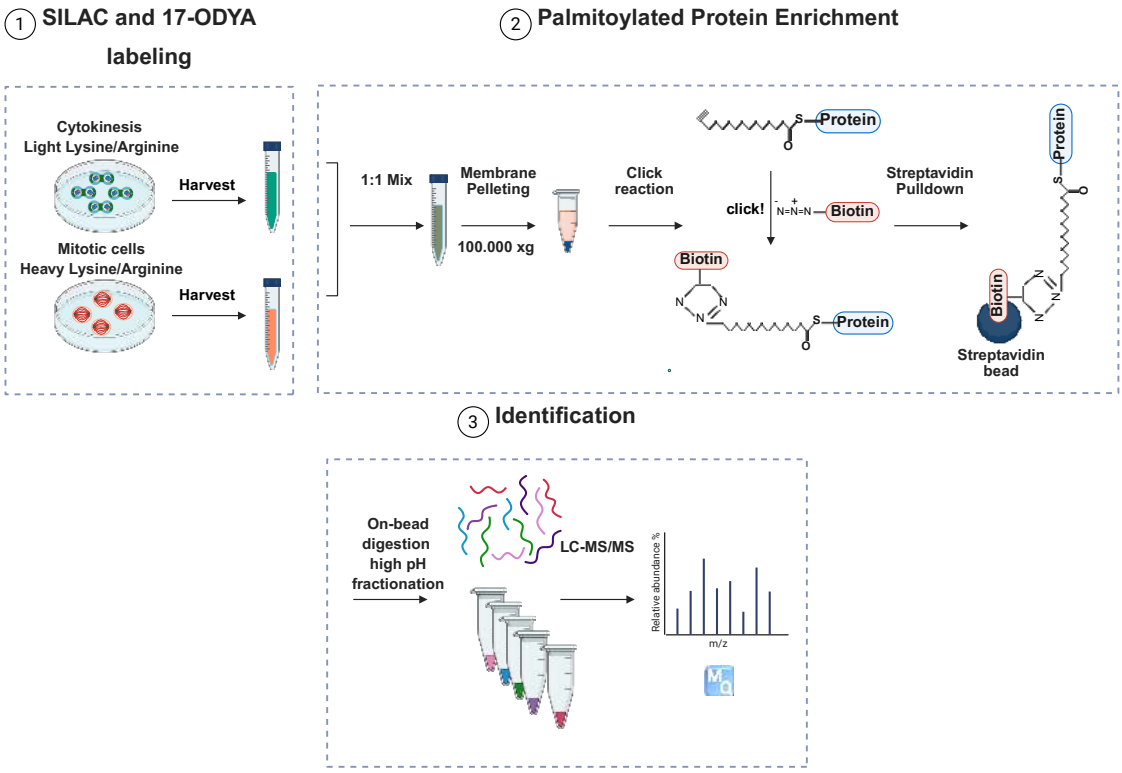

Figure 4.18: Workflow of SILAC-based palmitoyl-proteome analysis in mitotic and cytokinetic cells (Created with BioRender.com).

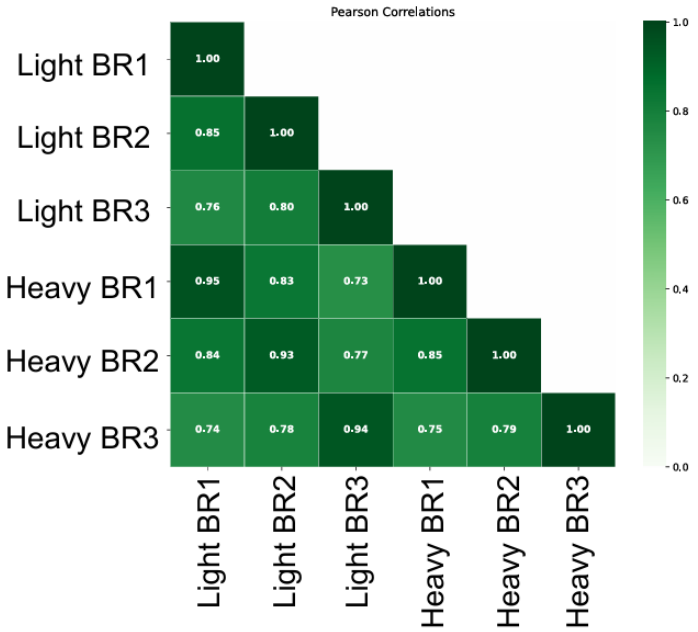

Figure 4.19: Pearson correlations of biological replicates SILAC labeled in mitosis and cytokinesis cells.

A significant enrichment of 109 proteins in cytokinesis and 83 in mitosis was identified among the 2,678 proteins that were quantified (Figure 4.20). In comparison to the interphase/mitosis comparison (23%), the percentage of significantly regulated proteins (7%) was significantly lower. Of these, 26% (50 proteins) had no prior evidence of palmitoylation, 4% (8 proteins) had experimentally confirmed palmitoylation, and 74% (140 proteins) had been previously identified in palmitoyl-proteome studies (Figure 4.20) .

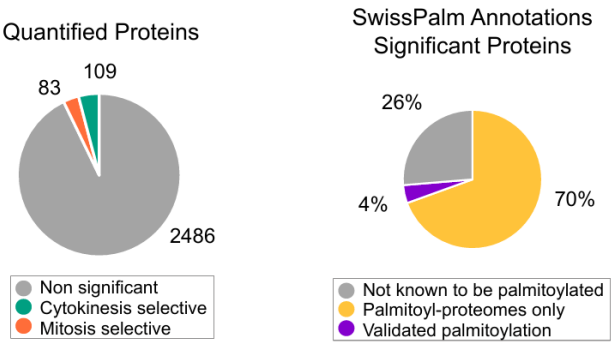

Figure 4.20: Distribution of quantified proteins by significance (left) and SwissPalm annotation status of significant proteins (right).

A volcano plot was generated to compare palmitoylation levels between mitosis and cytokinesis. Proteins were considered significantly different if their adjusted p-value was below 0.05 and their $\log_2$ fold change was greater than 1. Among these, it was discovered that 83 proteins were enriched in cytokinesis and 109 proteins were selectively palmitoylated during mitosis. Several well-known cell division regulators, including Ezrin and CEP55, were found among the significantly changed proteins.

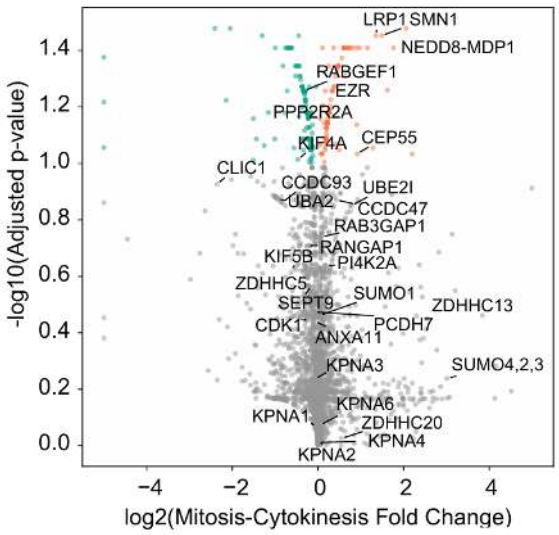

Figure 4.21: Volcano plot showing differentially palmitoylated proteins between mitosis and cytokinesis cells.

Proximity ligation assay (PLA) was performed to validate the palmitoylation of ezrin and palmitoylated ezrin localization in mitosis cells. Cells were metabolically labeled with 17-ODYA and then fixed. Following fixation, click chemistry was used to covalently attach a biotin tag to palmitoylated proteins. The samples were subsequently processed following the standard PLA protocol. After click chemistry-based biotin tagging of palmitoylated proteins, cells were incubated with primary antibodies targeting biotin and ezrin to enable detection of protein proximity signals.

The results (Figure 4.23) showed a significant increase in PLA signals per cell in the 17-ODYA-treated group compared to the control conditions. Control conditions, including the use of only biotin antibody, only ezrin antibody, or the substitution of 17-ODYA with palmitic acid, did not result in significant signal increases. These findings support the specificity and biological impacts of ezrin palmitoylation in mitosis. Furthermore, membrane-localized palmitoylated ezrin signals were also detected, indicating the spatial enrichment of this palmitoylation along the plasma membrane during mitosis (Figure 4.22).

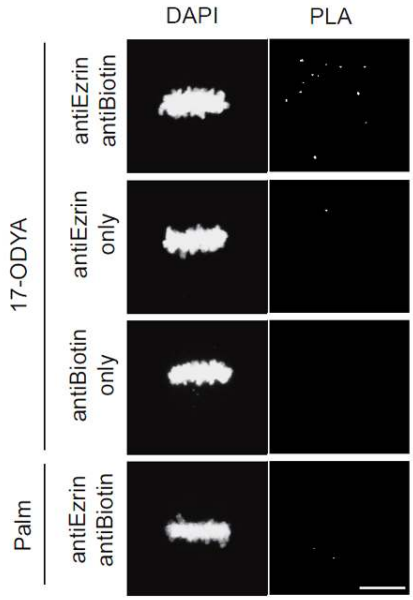

Figure 4.22: PLA detection of palmitoylated ezrin in mitotic HeLa cells. DAPI marks nuclei. Scale bar $=10\,\mu$m

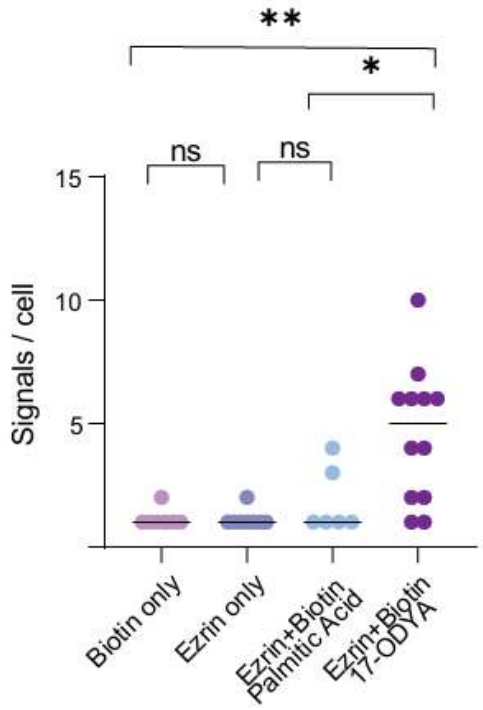

Figure 4.23: PLA-based detection of Ezrin palmitoylation.

Both datasets specific to mitosis and cytokinesis showed shared enrichment for membrane-bound organelles and exosomal compartments, according to gene ontology enrichment analysis of these highly regulated proteins. Protease-related proteins were selectively enriched in cytokinesis, while vesicle-associated proteins were preferentially enriched in mitosis (Figure 4.24). Mapping individual proteins to these enriched GO terms using gProfiler further indicated that, despite the vesicle-related term being selectively enriched in mitosis, a substantial number of early and recycling endosome-associated proteins were found among the cytokinesis-selective group. The significant representation of other GO categories, such as cadherin binding, suggests that palmitoylation may play a role in adhesion-related pathways (Figure 4.26). Interestingly, during cytokinesis, palmitoylation was selectively observed in most proteasome-related proteins. This suggests that palmitoylation may play a role in the proteasome-mediated breakdown of mitotic regulators as cells exit mitosis.

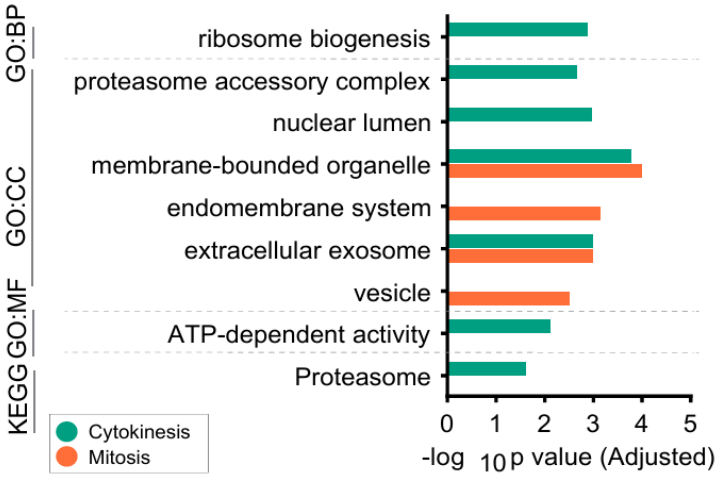

Figure 4.24: Enriched GO terms in palmitoylated proteins during mitosis and cytokinesis.

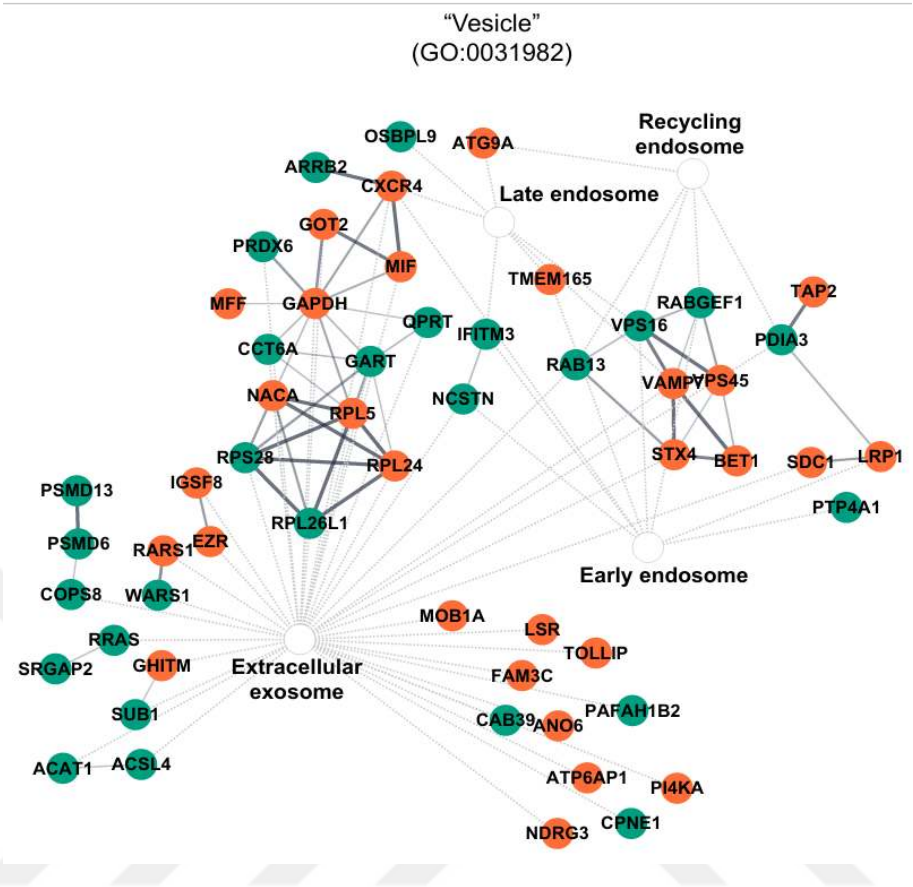

Figure 4.25: Network of palmitoylated proteins linked to the GO term "vesicle" (GO:0031982).

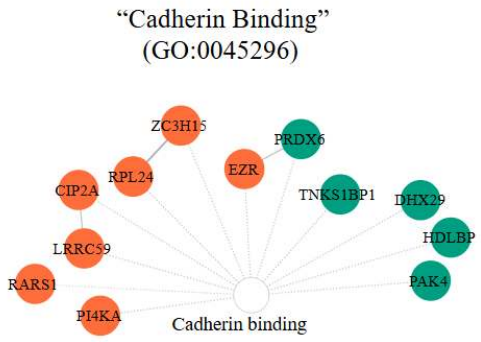

Figure 4.26: Network of palmitoylated proteins linked to the "cadherin binding" (GO:0045296).

4.4 Palmitoylation Clustering and Cross-Comparison with Phosphorylation

Palmitoylation patterns were systematically compared in interphase, mitosis, and cytokinesis to better understand how the regulation of protein palmitoylation occurs during cell division. All proteins measured in the SILAC-based dataset had their relative protein intensities in interphase and cytokinesis normalized to mitotic levels. Proteins that were consistently measured in the cell cycle were categorised according to the phase in which their palmitoylation levels were higher or lower (Figure 4.27).

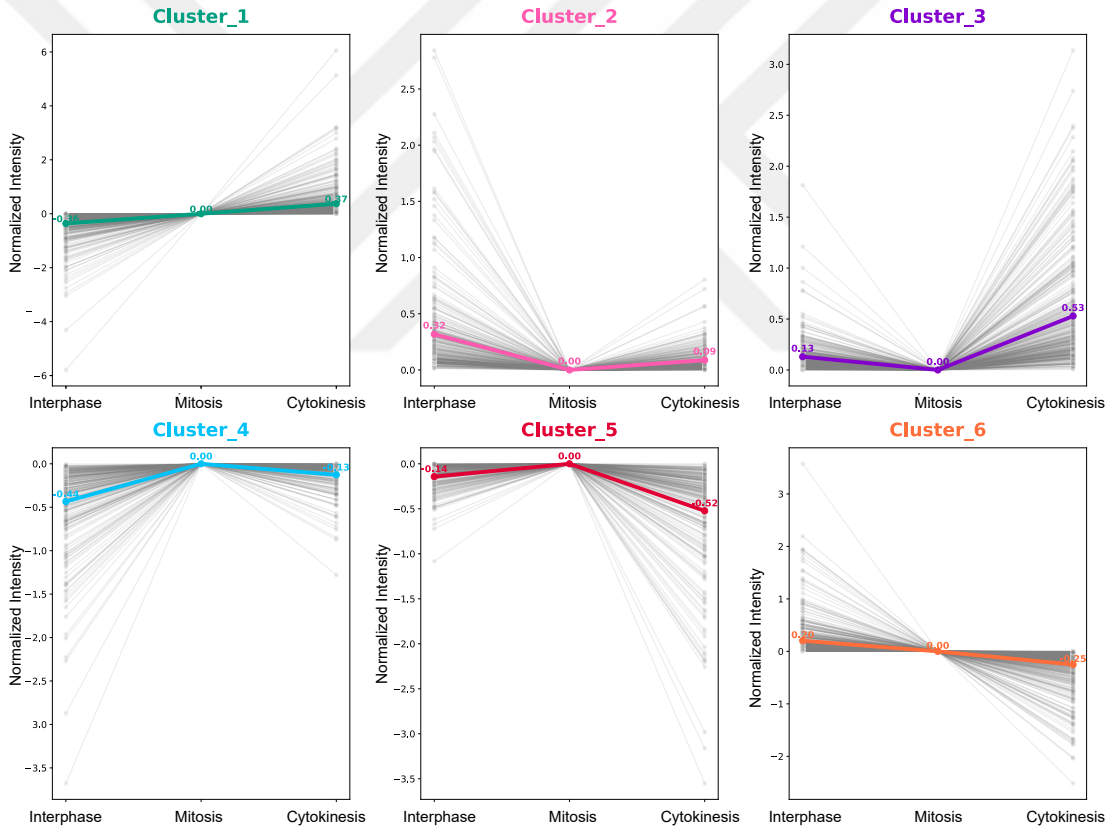

Figure 4.27: Clustering of palmitoylated proteins across interphase, mitosis, and cytokinesis.

After that, the DAVID platform was used to perform GO enrichment analysis on highly regulated proteins from each cluster. GO terms related to cell cycle processes are shown (Figure 4.28). In particular, clusters 2 and 3 that showed marked reduc-

tions in palmitoylation during mitosis were enriched for cell division-related terms, suggesting that a wave of depalmitoylation may accompany the mitotic phase. Nuclear membrane-related terms were selectively enriched in Cluster 5, which is defined by increased palmitoylation levels during mitosis. These results might suggest that palmitoylation promotes the breakdown of the nuclear envelope during mitosis.

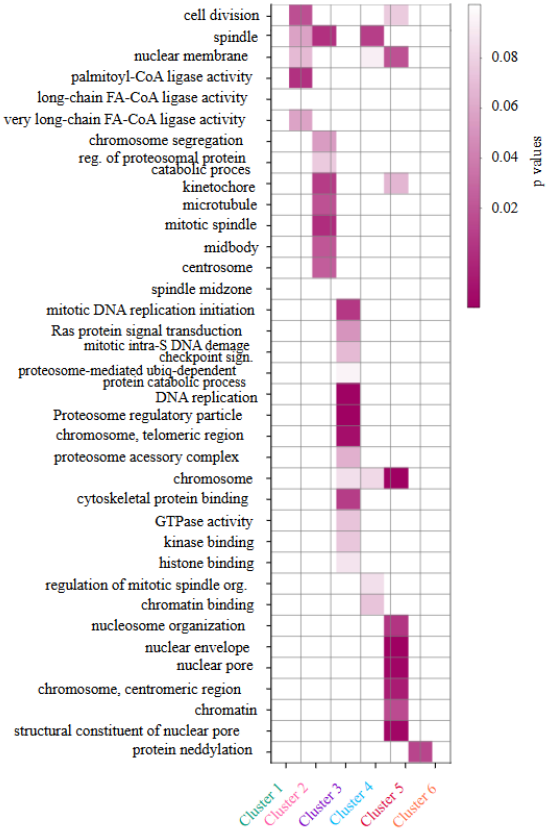

Figure 4.28: Functional annotation clustering of palmitoylated proteins across clusters using DAVID analysis.

For each cluster, the distribution of all measured proteins as well as the subset of proteins that were significantly regulated were analysed. Striped bars represents the quantified proteins and dotted bars represents the significantly regulated proteins (Figure4.27). Among them, Cluster 1 defined by a monotonic increase in palmitoylation from interphase to cytokinesis contained the largest proportion of significantly modulated proteins. The relationship between palmitoylation and phosphorylation

dynamics in the cell cycle cell division was evaluated by comparing the trends identified with phosphorylation profiles [Karayel et al., 2018]. Co-clustered proteins which exhibiting matching regulation patterns in both the palmitome and phosphoproteome were quantified and visualized (Figure 4.27, filled bars). Representative examples from each cluster that were chosen based on annotation in the SwissPalm database (Figure 4.29).

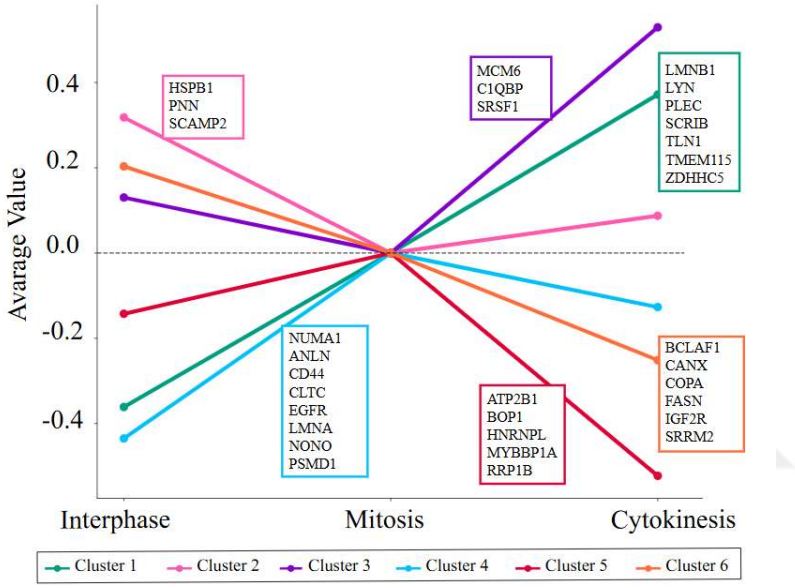

Figure 4.29: Average profiles of clustered palmitoylated proteins across cell cycle stages.

ZDHHC5 has been proposed as a potential contributor to disease-associated phosphorylation pathways. To gain further insight into its role, the distribution of phosphorylation sites along the ZDHHC5 protein sequence was examined. A total of 76 distinct phosphosites were identified. The extent of phosphorylation was found to vary across the sequence, and several residues were frequently modified. In particular, S406, S409 and S621 was previously identified [Karayel et al., 2018]. The ten most frequently phosphorylated residues are labeled, and the protein domains including the transmembrane regions (TM1-TM3) and the catalytic domain of DHHC5 are shown to provide structural context (Figure 4.30) [PhosphoSitePlus,

2025].

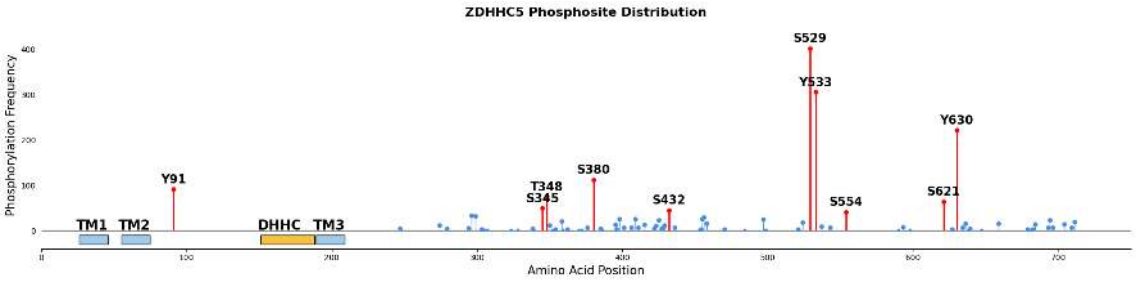

Figure 4.30: Phosphorylation sites on ZDHHC5. Vertical bars represent site frequency; top 10 sites are labeled in red. Protein domains (TM1–3, DHHC) are shown as colored boxes [PhosphoSitePlus, 2025]

Lastly, Cluster 1 containing the most significantly regulated proteins was examined in further detail. Among the 488 proteins in this cluster, 124 have significantly regulated in the cell cycle, and 53 of these shares the same regulation pattern in the phosphoproteome data. These overlapping proteins were found to be enriched for nuclear and cell junction components (Figure 4.31). The significance of palmitoylation changes is indicated by the colour gradient applied to the nodes in the network.

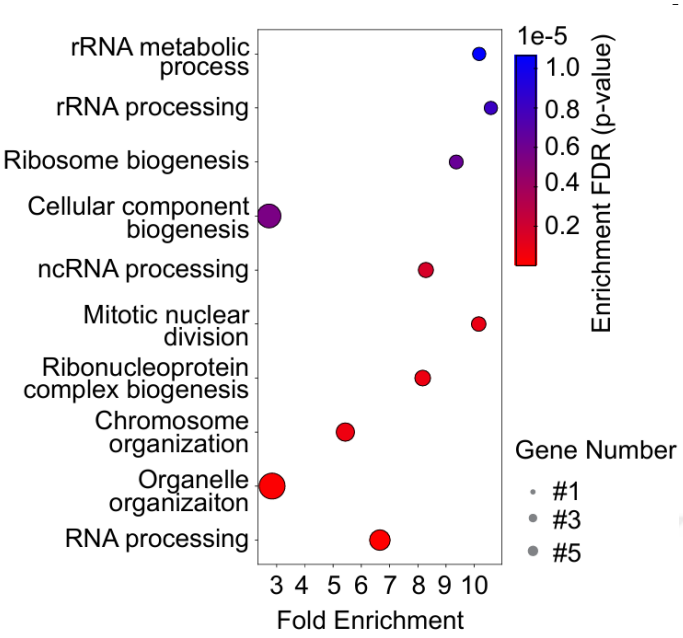

Figure 4.31: DAVID enrichment dot plot of overlapped clustered palmitoylated proteins in cluster 1.

4.5 ZDHHC5 Controls Mitotic Exit and Proteome Integrity During Cytokinesis

Palmitoylation is a reversible lipid modification that helps proteins attach to membranes and regulate their localization. ZDHHC5 is a membrane-localized palmitoyltransferase that, unlike most DHHC family members, resides at the plasma membrane [Ohno et al., 2006]. It has been associated with several cellular processes, including adhesion and trafficking [Woodley and Collins, 2019]. ZDHHC5 is a quantified protein in the SILAC mitosis cytokinesis data. Its expression profile followed a similar trend to other proteins regulated by phosphorylation and palmitoylation, as shown in clusters comparisons with phosphoproteomic data [Karayel et al., 2018].

The loss of ZDHHC5 disrupts the palmitoylation of PCDH7, thereby preventing its proper localization to the mitotic cell surface and cleavage. This mislocalization impairs the activation of myosin at the division site, leading to defects in cleavage furrow ingression and ultimately resulting in cytokinesis failure. The absence of ZDHHC5 results in more cells failing cytokinesis and becoming multinucleated [Özkan

et al., 2023].

These findings suggest that ZDHHC5 plays a broader role in organizing the mitotic cortex by directing palmitoylated proteins to specific membrane domains during division.

To identify which ZDHHC enzymes might play a role in cell division, a screening was performed by quantifying the percentage of multinucleated cells across 33 biological replicates. ZDHHC12 and ZDHHC13 significantly increased the percentage of multinucleated cells, which suggest a potential role in cell division failure. In contrast, multinucleation percentages of ZDHHC2, ZDHHC4, ZDHHC6, and ZDHHC24 were not significant, so they may not to be important for cell division (Figure 4.32).

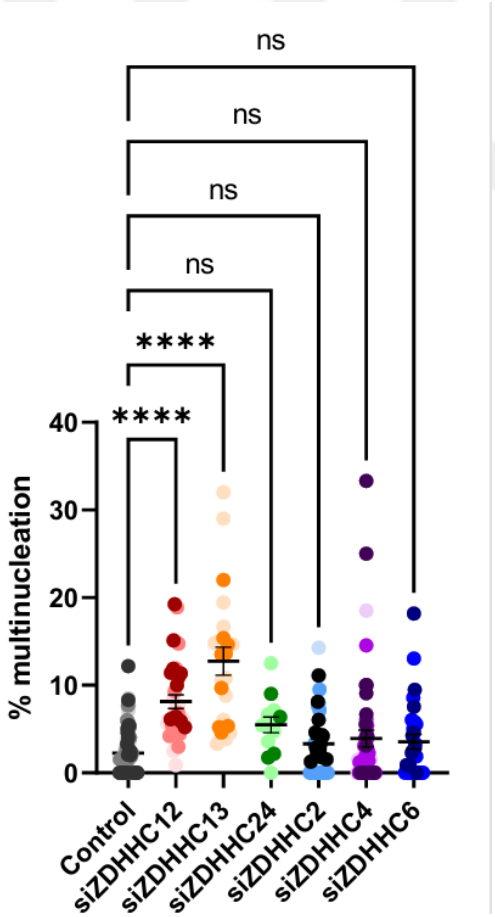

Figure 4.32: Multinucleation percentages upon siRNA-mediated knockdown of ZDHHC family members.

The screening for ZDHHC5, ZDHHC12, and ZDHHC13 was repeated. In a second experiment with three replicates, ZDHHC5, ZDHHC12, and ZDHHC13 again increased the number of multinucleated cells, confirming their relation with cell division machinery (Figure 4.33, 4.35, 4.34).

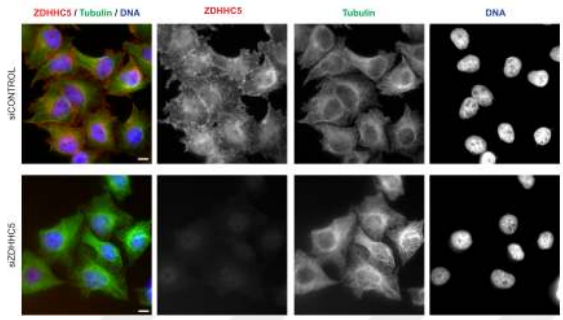

Figure 4.33: Immunofluorescence images showing *ZDHHC5* depletion.

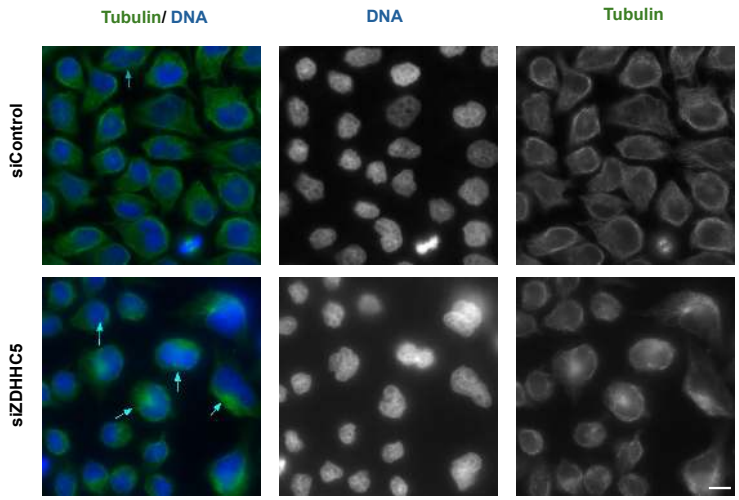

Figure 4.34: Multinucleation phenotype in siZDHHC5 cells visualized by tubulin (Green) and DNA (Blue) staining.

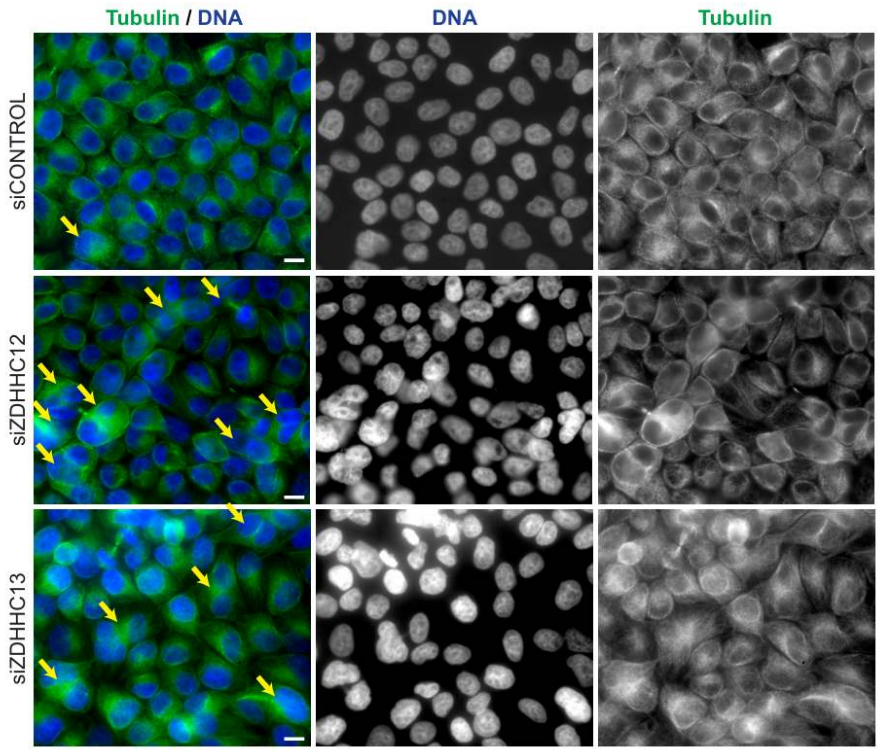

Figure 4.35: Multinucleation phenotype in siZDHHC2 and siZDHHC13 cells visualized by tubulin (Green) and DNA (Blue) staining.

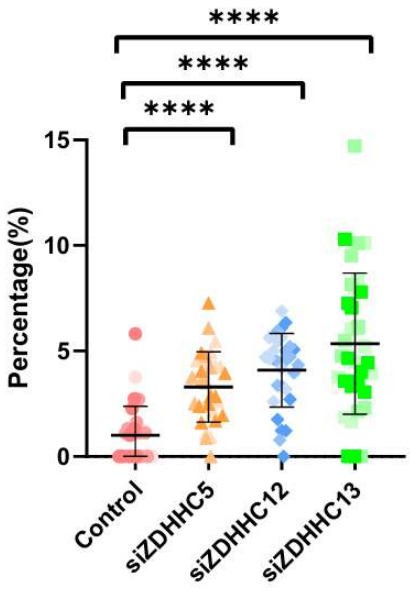

Figure 4.36: Multinucleation percetages upon knockdown of *ZDHHC5*, *ZDHHC12*, and *ZDHHC13*.

A ZDHHC5 KO cell line was generated to further investigate the role of ZDHHC5 in cell division. Live cell imaging experiments were performed using a Leica DMi8 widefield fluorescence microscope. Both brightfield and fluorescence channels were used to monitor dividing cells, and images were acquired every minute. For figure presentation, a single focal plane was selected from either single images or z-stacks acquired every 3 minutes. The duration of cell division was quantified by tracking individual cells over time (Figure 4.37). Non-targeting (sgNT) cells were used as a control for comparison.

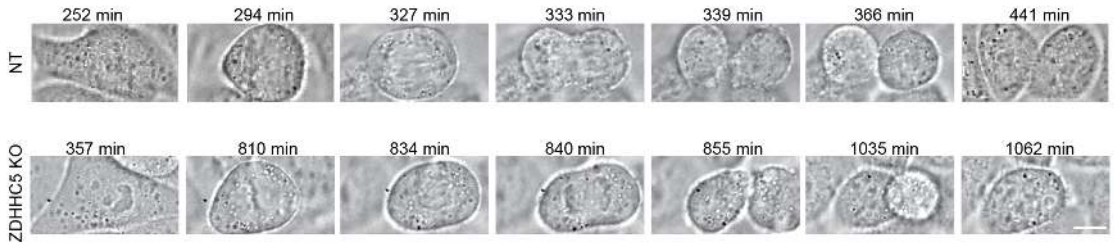

Figure 4.37: Time lapse images showing cell divison progression in control (NT) and *ZDHHC5* KO cells.

The duration from anaphase to abscission and from furrow ingression to abscission was significantly prolonged in ZDHHC5-KO cells compared to control (sgNT) cells. In cells lacking ZDHHC5, the time between anaphase and abscission, as well as between furrow ingression and abscission, was noticeably longer compared to control cells. These delays were highly significant (p ¡ 0.0001)(Figure 4.38). ZDHHC5 may have a role in the timely progression of late mitotic events, particularly during cytokinesis and abscission.

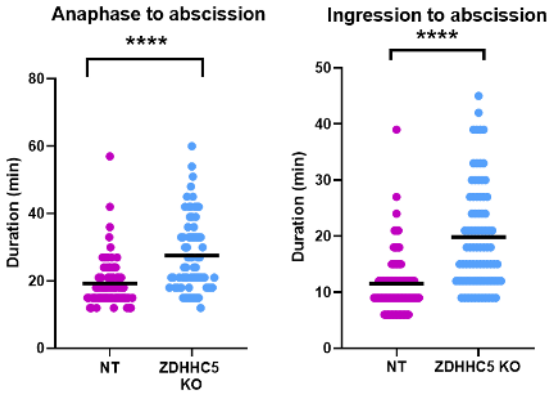

Figure 4.38: Quantification of mitotic exit duration in ZDHHC5 KO and control cells. A significant increase in duration was observed in KO cells (****, unpaired t-test).

A global proteomic analysis was performed in ZDHHC5 KO HeLa Kyoto cells

to assess the impact of ZDHHC5 loss on the cellular protein expression profile. ZDHHC5-KO cells generated using CRISPR/Cas9 technology were compared to non-targeting (NT) control cells.To determine at which stage of the cell cycle ZDHHC5 substrates are modified during cell division, we validated ZDHHC5 palmitoylation by Western blot in mitotic and cytokinetic cells. Our results showed that ZDHHC5 undergoes increased autopalmitoylation specifically during cytokinesis (Figure 4.39). Monopolar cytokinesis was induced by sequential treatment with STLC and Purvalanol A. Three biological replicates were prepared for each condition. After cell lysis, biotin labeling was carried out using click chemistry, followed by enrichment of biotinylated proteins with streptavidin beads. The samples were processed for LC-MS/MS analysis. As of this reporting period, three biological replicate and two technical replicate from each group has been analyzed by LC-MS/MS, and the resulting proteomic data have been evaluated.

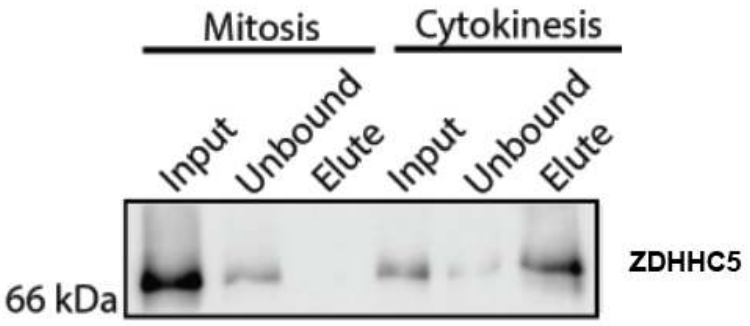

Figure 4.39: Western blot showing enrichment of palmitoylated ZDHHC5 in cytokinesis cells.

The data were analyzed using FragPipe, and unique peptides were included in the analysis. Following FragPipe analysis, the resulting protein lists were further processed in Perseus. For downstream statistical analysis, only proteins identified with unique peptide-spectrum matches (PSMs) were included to increase confidence in quantification. The comparison between ZDHHC5 KO and control (NT) cells was performed using a two-sample Student's t-test. p-values were calculated to identify

proteins that were significantly altered in response to ZDHHC5 KO.

The number of proteins identified in each biological replicate using FragPipe is represented (Tablo 4.3). In the *ZDHHC5* knockout (KO) group, the number of identified proteins ranged from 1644 to 1849, while in the NT control group, the counts ranged from 2038 to 2700. As expected, the number of identified proteins in the KO samples was slightly lower compared to the NT controls.

Table 4.3: Quantified protein numbers in Fragpipe.

Sample	**Identified Proteins**
KO BR1	1815
KO BR2	1644
KO BR3	1849
NT BR1	2038
NT BR2	2700
NT BR3	2187

To check how similar the biological replicates are, Pearson correlation coefficients were calculated for both the NT and KO groups using unique PSM values. As shown in the heatmaps, all replicate pairs within each group exhibited high correlation $r > 0.83$. Interestingly, the KO samples showed slightly higher pairwise correlations (ranging from 0.854 to 0.863) compared to the NT samples (ranging from 0.834 to 0.846). These results show that the proteome profiles are consistent across replicates in KO and NT samples (Figure 4.40).

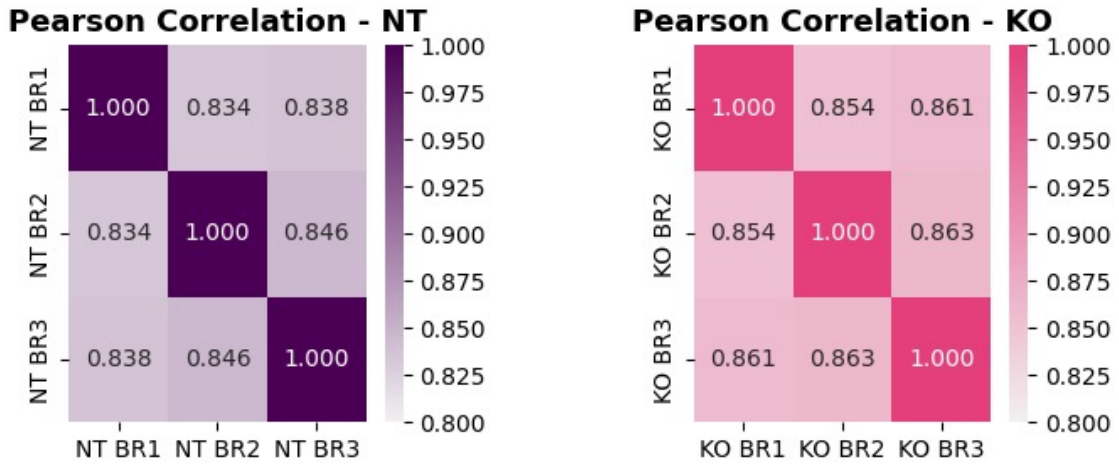

(a) Pearson correlation among NT biological replicates.

(b) Pearson correlation among KO biological replicates.

Figure 4.40: Pearson correlation heatmaps showing reproducibility across biological replicates in NT and KO groups.

PCA was performed to visualize the overall variation in the proteomic datasets (Figure 4.41). The biological replicates from the NT and KO groups formed clusters, indicating intra-group consistency and separation between the two conditions.

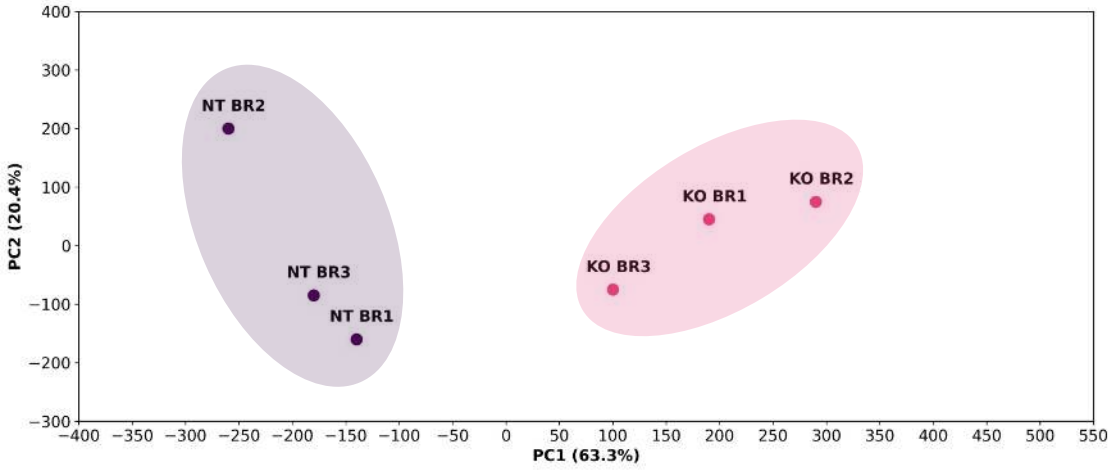

Figure 4.41: Principal component analysis of proteomic profiles in ZDHHC5 KO and sgNT samples.

Unique spectral counts were plotted to evaluate the consistency of the data (Figure 4.42). Within both the KO and control groups, all replicates overlapped distributions, suggesting a high level of similarity in protein detection and quantification between biological replicates.

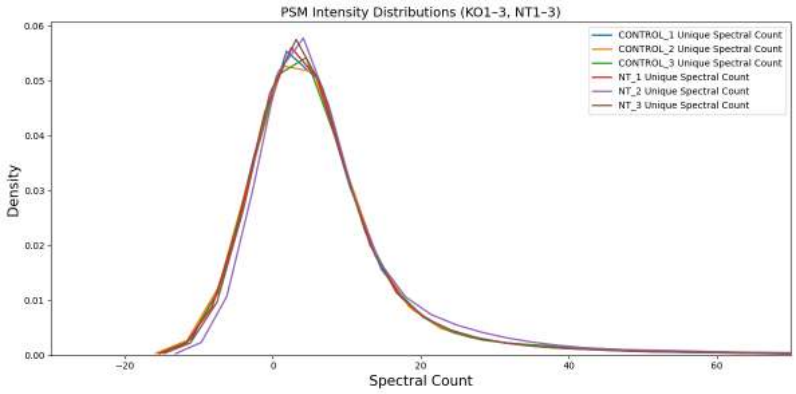

Figure 4.42: Unique spectral count density distribution in all biological replicates.

A volcano plot was generated to visualize differentially expressed proteins between ZDHHC5 knockout and sgNT control cells (Figure 4.43). Statistical significance (–log p-value) was plotted against log fold change values. Many proteins were significantly upregulated in the sgNT condition (pink) (Figure 4.43. In particular, several mitotic regulators, including MKI67, KIF23, TPX2, and INCENP, were among the proteins with the most significant decrease. The loss of ZDHHC5 can alter key pathways that govern mitotic progression and cytokinesis.

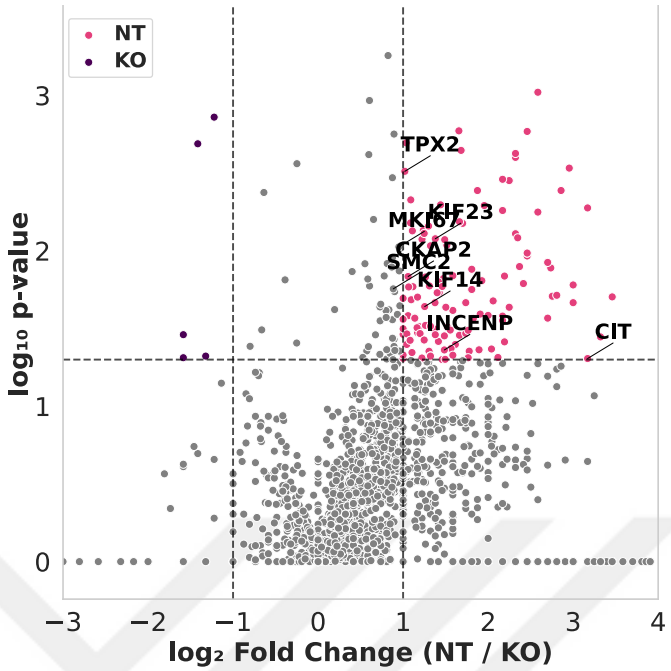

Figure 4.43: Volcano plot of differentially expressed proteins in *ZDHHC5* KO versus NT.

Chapter 5

DISCUSSION

This thesis is the first systematic and large scale investigations of protein palmitoylation in cell division. Palmitoylation is dynamically regulated in interphase , mitosis and cytokinesis in combination with a bioorthogonal palmitoylation labeling approach and *loss of function* analysis. The cooperative regulation of cytokinesis by distinct post-translational modifications including lipidation, phosphorylation, and ubiquitinationhas been further supported by our findings. Lipidation, phosphorylation, and ubiquitination have been shown to work together to regulate membrane remodeling, cytoskeletal organization, and the timing of cytokinesis [Bohnert and Gould, 2011].

Significant differences were seen in palmitoylation profiles between cytokinesis, mitosis, and interphase. Chromosome segregation, vesicle-mediated transport, and cleavage plane specification were the main processes associated with mitosis-enriched palmitoylated proteins, while interphase-enriched proteins were more likely to be responsible for membrane scaffolding and nuclear envelope organization. The accumulation of PIP at the cleavage furrow during cytokinesis corresponds with the positioning of various palmitoylated proteins, emphasizing coordination between lipid signaling and reversible acylation [Atilla-Gokcumen et al., 2014].

The palmitoyl acyltransferase ZDHHC5 has been identified as a key cytokinesis mediator. Both RNAi-mediated and CRISPR-based knockouts of ZDHHC5 resulted in significant division abnormalities, including as extended cytokinesis, increased multinucleation, and incomplete furrow ingression. Phenotypes demonstrate how ZDHHC5 regulates actomyosin ring dynamics and membrane trafficking. Since their silencing resulted in comparable abnormalities, ZDHHC12 and ZDHHC13 also remained out as significant possibilities, indicating possible redundancy function across ZDHHC enzymes. ZDHHC5 has previously been linked to the palmitoylation and

mitotic localization of PCDH7, a modification that promotes cortical contractility and supports the progression of the cleavage furrow [Özkan et al., 2023].

Remarkably, our SILAC-based results showed that palmitoylated proteins were concentrated in proteasomal and ribosomal components during cytokinesis. This observation suggests spatial regulation of localized translation and protein breakdown. These processes may be coordinated within specific cellular compartments via reversible lipidation. This type of compartmentalized regulation is necessary for cytokinesis to be executed precisely [Bohnert and Gould, 2011].

Additionally, the dataset revealed significant interaction between phosphorylation and palmitoylation. Numerous mitotic proteins were shown to be altered by both post-translational modifications using cluster-based analysis, suggesting that a coordinated or sequential process may be used to control the time of division and spatial organization. Because of their complementary functions in promoting contractile ring assembly, actomyosin cortex stabilization, and membrane remodeling, post-translational modifications have been identified as a key mechanism in the spatial and temporal regulation of cytokinesis [Bohnert and Gould, 2011], [Alonso-Matilla et al., 2024].

This study further confirmed palmitoylation of ezrin during mitosis. Following 17-ODYA administration during mitosis, a PLA demonstrated a prominent localization along the plasma membrane and a considerable increase in palmitoylated ezrin signals per cell. The specificity of the alteration was confirmed by the lack of equivalent signals under control settings, such as using only one main antibody or replacing 17-ODYA with palmitic acid. This result is consistent with earlier research showing that palmitoylation promotes the recruitment of signaling proteins to membrane microdomains, allowing them to interact with ezrin for cytoskeletal anchoring, as shown in the context of Fas signaling [Feig et al., 2007]. Since ezrin is known to connect the plasma membrane to the actin cytoskeleton during cortical remodeling and furrow ingression, it is hypothesized that its mitotic-specific palmitoylation serves as a spatiotemporal regulatory mechanism that enriches ezrin at the exact location and time that cytoskeletal coordination is needed.

Additionally, recent research has demonstrated that acetyl-CoA carboxylase inhi-

bition results in spindle aberrations and impaired tubulin palmitoylation, suggesting a functional connection between lipid metabolism and mitotic microtubule dynamics [Fang et al., 2023]. These results support the idea that lipid changes have more than only structural roles in the regulation of the mitotic machinery.

During cell division, palmitoylation is positioned as a crucial post-translational alteration that is both functionally and temporally regulated. ZDHHC5, ZDHHC12, and ZDHHC13 are important palmitoyltransferases that are involved in coordinating the membrane-cytoskeleton interactions required for mitotic progression and effective cytokinesis. These results highlight the significance of reversible lipid changes in providing precise spatial and temporal control during division, especially when paired with new discoveries about lipid-mediated mechanical regulation at the cytokinetic furrow [Alonso-Matilla et al., 2024]. More research is necessary to determine whether dysregulated palmitoylation contributes to the mitotic abnormalities seen in proliferative diseases.

Phosphorylation of ZDHHC5 at S406, S409 and S621, has previously been identified as a cell cycle associated modification [Karayel et al., 2018]. In the present study, palmitoylation of ZDHHC5 was found to be similarly upregulated during cytokinesis, suggesting that these two post translational events may be regulated in parallel. S621 is located within the C-terminal region of ZDHHC5, which is known to contain multiple regulatory elements [Plain et al., 2020]. ZDHHC5 activity can be modulated by phosphorylation, as demonstrated by the inhibitory effect of Y91 phosphorylation on enzymatic function [Woodley and Collins, 2021]. Although the specific role of S621 phosphorylation remains to be determined, the observed temporal overlap with palmitoylation raises the possibility of coordinated control. It is therefore possible that phosphorylation at S621 may contribute to the spatial or temporal tuning of ZDHHC5 activity during cytokinesis, either directly or through cross-regulation with palmitoylation.

One of the proteins that showed downregulation in *ZDHHC5* KO cells was INCENP. This protein plays an important role in the final steps of mitosis and cytokinesis. It is part of a group of proteins that help chromosomes separate properly and assist in completing cell division. A recent study has suggested that INCENP

is palmitoylated by ZDHHC5 [Zhang et al., 2021]. This type of modification helps proteins attach to membranes and carry out their functions in specific cellular locations. When the ZDHHC5 depleted, It might not function properly during cytokinesis. This may emphasize why *ZDHHC5* knockout cells show problems such as prolonged division and the presence of multiple nuclei. These findings support the idea that ZDHHC5 may regulate important cytokinesis proteins like INCENP through palmitoylation.

In general, the findings presented in this study indicate that palmitoylation is actively regulated during cell division, rather than a static lipid modification. Its timing and localization particularly through the activity of enzymes such as ZDHHC5 were found to be critical to the proper progression of mitosis and cytokinesis. As accurate cell division is required to maintain genomic stability, any disruption in these regulatory mechanisms may lead to adverse outcomes. In particular, dysregulated palmitoylation has been associated with uncontrolled cell proliferation, a hallmark of many cancers. By uncovering how palmitoylation is controlled during cell division, this work provides a foundation for future studies that aim to better understand the molecular causes of proliferative diseases and explore potential therapeutic targets.

BIBLIOGRAPHY

[Alonso-Matilla et al., 2024] Alonso-Matilla, R., Lam, A. R., and Miettinen, T. P. (2024). Cell-intrinsic mechanical regulation of plasma membrane accumulation at the cytokinetic furrow. *Proceedings of the National Academy of Sciences*, 121(29):e2320769121.

[Atilla-Gokcumen et al., 2014] Atilla-Gokcumen, G. E., Muro, E., Relat-Goberna, J., Sasse, S., Bedigian, A., Coughlin, M. L., Garcia-Manyes, S., and Eggert, U. S. (2014). Dividing cells regulate their lipid composition and localization. *Cell*, 156(3):428–439.

[Bohnert and Gould, 2011] Bohnert, K. A. and Gould, K. L. (2011). On the cutting edge: post-translational modifications in cytokinesis. *Trends in cell biology*, 21(5):283–292.

[Brownlee and Heald, 2019] Brownlee, C. and Heald, R. (2019). Importin α partitioning to the plasma membrane regulates intracellular scaling. *Cell*, 176(4):805–815.

[Chamberlain and Shipston, 2015] Chamberlain, L. H. and Shipston, M. J. (2015). The physiology of protein s-acylation. *Physiological reviews*, 95(2):341–376.

[Champion et al., 2017] Champion, L., Linder, M. I., and Kutay, U. (2017). Cellular reorganization during mitotic entry. *Trends in cell biology*, 27(1):26–41.

[CHOPCHOP Team, 2025] CHOPCHOP Team (2025). CHOPCHOP — CRISPR sgRNA design web tool. `https://chopchop.cbu.uib.no`. Erişim tarihi: 1 Temmuz 2025.

[Chung et al., 2025] Chung, C., Tang, Y., Chiu, Y., Li, S., Hsieh, W., Yao, L., Chiang, Y., Pang, Y., Chen, G., Chou, K., Paik, Y., Tran, P., Lin, C., Kao, Y., Chen, Y., Chang, W., Hsu, J., Horng, J., and Lee, T. (2025). Dbptm 2025 update: Comprehensive integration of ptms and proteomic data for advanced insights into cancer research. *Nucleic Acids Research*, 53(D1):D377–D386.

[Conibear and Davis, 2010] Conibear, E. and Davis, N. G. (2010). Palmitoylation and depalmitoylation dynamics at a glance. *Journal of cell science*, 123(23):4007–4010.

[Draper and Smith, 2009] Draper, J. M. and Smith, C. D. (2009). Palmitoyl acyltransferase assays and inhibitors. *Molecular membrane biology*, 26(1-2):5–13.

[Fang et al., 2023] Fang, C.-T., Kuo, H.-H., Amartuvshin, O., Hsu, H.-J., Liu, S.-L., Yao, J.-S., and Yih, L.-H. (2023). Inhibition of acetyl-coa carboxylase impaired tubulin palmitoylation and induced spindle abnormalities. *Cell Death Discovery*, 9(1):4.

[Feig et al., 2007] Feig, C., Tchikov, V., Schütze, S., and Peter, M. E. (2007). Palmitoylation of cd95 facilitates formation of sds-stable receptor aggregates that initiate apoptosis signaling. *The EMBO journal*, 26(1):221–231.

[Gök et al., 2020] Gök, C., Plain, F., Robertson, A. D., Howie, J., Baillie, G. S., Fraser, N. J., and Fuller, W. (2020). Dynamic palmitoylation of the sodium-calcium exchanger modulates its structure, affinity for lipid-ordered domains, and inhibition by xip. *Cell reports*, 31(10).

[Greaves and Chamberlain, 2011] Greaves, J. and Chamberlain, L. H. (2011). Dhhc palmitoyl transferases: substrate interactions and (patho) physiology. *Trends in biochemical sciences*, 36(5):245–253.

[Hannoush and Arenas-Ramirez, 2009] Hannoush, R. N. and Arenas-Ramirez, N. (2009). Imaging the lipidome: ω-alkynyl fatty acids for detection and cellular visualization of lipid-modified proteins. *ACS chemical biology*, 4(7):581–587.

[Karayel et al., 2018] Karayel, Ö., Şanal, E., Giese, S. H., Üretmen Kagıalı, Z. C., Polat, A. N., Hu, C.-K., Renard, B. Y., Tuncbag, N., and Özlü, N. (2018). Comparative phosphoproteomic analysis reveals signaling networks regulating monopolar and bipolar cytokinesis. *Scientific Reports*, 8(1):2269.

[Ko et al., 2019] Ko, P.-J., Woodrow, C., Dubreuil, M. M., Martin, B. R., Skouta, R., Bassik, M. C., and Dixon, S. J. (2019). A zdhhc5-golga7 protein acyltransferase complex promotes nonapoptotic cell death. *Cell chemical biology*, 26(12):1716–1724.

[Leguay et al., 2022] Leguay, K., Decelle, B., Elkholi, I. E., Bouvier, M., Côté, J.-F., and Carréno, S. (2022). Interphase microtubule disassembly is a signaling cue that drives cell rounding at mitotic entry. *Journal of Cell Biology*, 221(6):e202109065.

[Lemonidis et al., 2015] Lemonidis, K., Werno, M. W., Greaves, J., Diez-Ardanuy, C., Sanchez-Perez, M. C., Salaun, C., Thomson, D. M., and Chamberlain, L. H. (2015). The zdhhc family of s-acyltransferases. *Biochemical Society transactions*, 43(2):217–221.

[Li et al., 2010] Li, Y., Hu, J., Höfer, K., Wong, A. M., Cooper, J. D., Birnbaum, S. G., Hammer, R. E., and Hofmann, S. L. (2010). Dhhc5 interacts with pdz domain 3 of post-synaptic density-95 (psd-95) protein and plays a role in learning and memory. *Journal of Biological Chemistry*, 285(17):13022–13031.

[Linder and Deschenes, 2007] Linder, M. E. and Deschenes, R. J. (2007). Palmitoylation: policing protein stability and traffic. *Nature reviews Molecular cell biology*, 8(1):74–84.

[Morgan, 2007] Morgan, D. O. (2007). *The cell cycle: principles of control*. New science press.

[Nigg, 1993] Nigg, E. A. (1993). Targets of cyclin-dependent protein kinases. *Current opinion in cell biology*, 5(2):187–193.

[Ohno et al., 2006] Ohno, Y., Kihara, A., Sano, T., and Igarashi, Y. (2006). Intracellular localization and tissue-specific distribution of human and yeast dhhc cysteine-rich domain-containing proteins. *Biochimica et Biophysica Acta (BBA)-Molecular and Cell Biology of Lipids*, 1761(4):474–483.

[Olsen et al., 2010] Olsen, J. V., Vermeulen, M., Santamaria, A., Kumar, C., Miller, M. L., Jensen, L. J., Gnad, F., Cox, J., Jensen, T. S., Nigg, E. A., et al. (2010). Quantitative phosphoproteomics reveals widespread full phosphorylation site occupancy during mitosis. *Science signaling*, 3(104):ra3–ra3.

[Özkan et al., 2023] Özkan, N. E., Yigit, B. N., Degirmenci, B. S., Qureshi, M. H., Yapici, G. N., Kamacıoglu, A., Bavili, N., Kiraz, A., and Ozlu, N. (2023). Cell cycle-dependent palmitoylation of protocadherin 7 by zdhhc5 promotes successful cytokinesis. *Journal of Cell Science*, 136(6):jcs260266.

[Özlü et al., 2015] Özlü, N., Qureshi, M. H., Toyoda, Y., Renard, B. Y., Mollaoglu, G., Özkan, N. E., Bulbul, S., Poser, I., Timm, W., Hyman, A. A., et al. (2015). Quantitative comparison of a human cancer cell surface proteome between interphase and mitosis. *The EMBO journal*, 34(2):251–265.

[Petronczki et al., 2008] Petronczki, M., Lénárt, P., and Peters, J.-M. (2008). Polo on the rise—from mitotic entry to cytokinesis with plk1. *Developmental cell*, 14(5):646–659.

[PhosphoSitePlus, 2025] PhosphoSitePlus (2025). Zdhhc5 protein – phosphositeplus. Accessed: 2025-08-06.

[Plain et al., 2020] Plain, F., Howie, J., Kennedy, J., Brown, E., Shattock, M. J., Fraser, N. J., and Fuller, W. (2020). Control of protein palmitoylation by regulating substrate recruitment to a zdhhc-protein acyltransferase. *Communications biology*, 3(1):411.

[Ramazi and Zahiri, 2021] Ramazi, S. and Zahiri, J. (2021). Post-translational

modifications in proteins: resources, tools and prediction methods. *Database*, 2021:baab012.

[Rega et al., 2025] Rega, C., Tsitsa, I., Roumeliotis, T. I., Krystkowiak, I., Portillo, M., Yu, L., Vorhauser, J., Pines, J., Mansfeld, J., Choudhary, J., et al. (2025). High resolution profiling of cell cycle-dependent protein and phosphorylation abundance changes in non-transformed cells. *Nature Communications*, 16(1):2579.

[Rocks et al., 2010] Rocks, O., Gerauer, M., Vartak, N., Koch, S., Huang, Z.-P., Pechlivanis, M., Kuhlmann, J., Brunsveld, L., Chandra, A., Ellinger, B., et al. (2010). The palmitoylation machinery is a spatially organizing system for peripheral membrane proteins. *Cell*, 141(3):458–471.

[Sergeeva and van der Goot, 2019] Sergeeva, O. A. and van der Goot, F. G. (2019). Anthrax toxin requires zdhhc5-mediated palmitoylation of its surface-processing host enzymes. *Proceedings of the National Academy of Sciences*, 116(4):1279–1288.

[Stypulkowski et al., 2018] Stypulkowski, E., Asangani, I. A., and Witze, E. S. (2018). The depalmitoylase apt1 directs the asymmetric partitioning of notch and wnt signaling during cell division. *Science signaling*, 11(511):eaam8705.

[Wang et al., 2023] Wang, L., Cai, J., Zhao, X., Ma, L., Zeng, P., Zhou, L., Liu, Y., Yang, S., Cai, Z., Zhang, S., et al. (2023). Palmitoylation prevents sustained inflammation by limiting nlrp3 inflammasome activation through chaperone-mediated autophagy. *Molecular Cell*, 83(2):281–297.

[Woodley and Collins, 2019] Woodley, K. T. and Collins, M. O. (2019). S-acylated golga7b stabilises dhhc 5 at the plasma membrane to regulate cell adhesion. *EMBO reports*, 20(10):e47472.

[Woodley and Collins, 2021] Woodley, K. T. and Collins, M. O. (2021). Regulation and function of the palmitoyl-acyltransferase zdhhc5. *The FEBS Journal*, 288(23):6623–6634.

[Yuan et al., 2024] Yuan, Y., Li, P., Li, J., Zhao, Q., Chang, Y., and He, X. (2024). Protein lipidation in health and disease: molecular basis, physiological function and pathological implication. *Signal Transduction and Targeted Therapy*, 9(1):60.

[Zhang et al., 2021] Zhang, Y., Li, F., Fu, K., Liu, X., Lien, I.-C., and Li, H. (2021). Potential role of s-palmitoylation in cancer stem cells of lung adenocarcinoma. *Frontiers in cell and developmental biology*, 9:734897.